White Rose Research Online

eprints@whiterose.ac.uk
https://eprints.whiterose.ac.uk
Universities of Leeds, Sheffield and York

Deposited via The University of York.

White Rose Research Online URL for this paper:
https://eprints.whiterose.ac.uk/id/eprint/174682/

Version: Accepted Version

Article:
Gibson, Kieran, Horvath, Laszlo, Maggi, C. F. et al. (2021) Isotope dependence of the type I ELMy H-mode pedestal in JET-ILW hydrogen and deuterium plasmas. Nuclear Fusion. 046015. ISSN: 1741-4326

https://doi.org/10.1088/1741-4326/abdd77

Reuse
This article is distributed under the terms of the Creative Commons Attribution-NonCommercial-NoDerivs (CC BY-NC-ND) licence. This licence only allows you to download this work and share it with others as long as you credit the authors, but you can't change the article in any way or use it commercially. More information and the full terms of the licence here: https://creativecommons.org/licenses/

Takedown
If you consider content in White Rose Research Online to be in breach of UK law, please notify us by emailing eprints@whiterose.ac.uk including the URL of the record and the reason for the withdrawal request.

UNIVERSITY OF LEEDS
University of Sheffield
UNIVERSITY of York

Isotope dependence of the type I ELMy H-mode pedestal in JET-ILW Hydrogen and Deuterium plasmas

L. Horvath[1,2], C.F. Maggi[1], A. Chankin[3], S. Saarelma[1], A.R. Field[1], S. Aleiferis[4], E. Belonohy[1], A. Boboc[1], G. Corrigan[1], E.G. Delabie[5], J. Flanagan[1], L. Frassinetti[6], C. Giroud[1], D. Harting[1], D. Keeling[1], D. King[1], M. Maslov[1], G.F. Matthews[1], S. Menmuir[1], S.A. Silburn[1], J. Simpson[1,7], A.C.C Sips[8,9], H. Weisen[10], K.J. Gibson[2] and JET Contributors*

EUROfusion Consortium, JET, Culham Science Centre, Abingdon OX14 3DB, UK
[1]CCFE, Culham Science Centre, Abingdon, OX14 3DB, UK
[2]York Plasma Institute, Department of Physics, University of York, York, YO10 5DD, UK
[3]Max-Planck-Institut für Plasmaphysik, Boltzmannstrasse 2, D-85748, Garching, Germany
[4]Institute of Nuclear & Radiological Sciences and Technology, Energy & Safety, NCSR Demokritos, Athens 15310, Greece
[5]Oak Ridge National Laboratory, Oak Ridge, Tennessee, United States of America
[6]Division of Fusion Plasma Physics, KTH Royal Institute of Technology, Stockholm, Sweden
[7]Aalto University, 02150 Espoo, Finland
[8]JET Exploitation Unit, Culham Science Centre, Abingdon, OX14 3DB, UK
[9]European Commission, Brussels, Belgium
[10]Swiss Plasma Center, Ecole Polytechnique Federale de Lausanne, Switzerland
*See the author list of E. Joffrin et al. 2019 Nucl. Fusion 59 112021

E-mail: laszlo.horvath@ukaea.uk

Abstract.

The pedestal structure, edge transport and linear MHD stability have been analysed in a series of JET-ILW Hydrogen (H) and Deuterium (D) type I ELMy H-mode plasmas. The pedestal pressure is typically higher in D than in H at the same input power and gas rate, with the difference mainly due to lower density in H than in D [1]. A power balance analysis of the pedestal has shown that higher inter-ELM separatrix loss power is required in H than in D to maintain a similar pedestal top pressure. This is qualitatively consistent with a set of interpretative EDGE2D-EIRENE simulations for H and D plasmas showing that higher edge particle and heat transport coefficients are needed in H than in D to match the experimental profiles. It has also been concluded that the difference in neutral penetration between H and D leads only to minor changes in the upstream density profiles and with trends opposite to experimental observations. This implies that neutral penetration has a minor role in setting the difference between H and D pedestals, but higher ELM and/or inter-ELM transport and pedestal stability are likely to be the main players. The interpretative EDGE2D-

EIRENE simulations, with simultaneous upstream and outer divertor target profile constraints, have indicated higher separatrix electron temperature in H than in D for a pair of discharges at low fuelling gas rate and similar stored energy (which required higher input power in H than in D at the same gas rate). The isotope dependence of linear MHD pedestal stability has been found to be small, but if a higher separatrix temperature is considered in H than in D, this could lead to destabilisation of Peeling-Ballooning modes and shrinking of the stability boundary, qualitatively consistent with the reduced pedestal confinement in H.

1. Introduction

Unravelling the isotope dependence of plasma confinement and transport would improve our ability to predict the performance of JET and ITER plasmas with deuterium-tritium (DT) mixture. The foreseen plasma scenario for these experiments is H-mode [2], where the level of energy and particle transport at the plasma edge is reduced and a steep pressure gradient is formed, which gives rise to a pressure pedestal. Although positive isotope mass scaling of the thermal energy confinement time in H-mode plasmas has been observed in several tokamaks such as JET [1], JT-60U [3, 4, 5], DIII-D [6] and ASDEX-Upgrade [7, 8, 9], this favourable isotope dependence has not yet been fully understood theoretically. The favourable isotope scaling has also been found in L-mode plasmas, but is generally found to be weaker than in H-modes [1, 8, 10, 11, 12, 13]. Furthermore, stellarators are also exhibit a favourable isotope scaling [14, 15].

H-mode experiments in JET with the carbon wall (JET-C) with different hydrogen isotopes showed virtually no isotope dependence of the thermal energy confinement time in plasmas at similar density: $\tau_{\mathrm{E,th}} \propto A^{0.03}$, where A is the mass number of the main ion ($A = m_{\mathrm{ion}}/m_{\mathrm{proton}}$) [16]. The strong positive isotope dependence of the pedestal stored energy was compensated with a weak negative isotope dependence of the core plasma [16]. A possible explanation for the low exponent is due to the collinearity of the density and mass dependence in the dataset. This is confirmed by a recent analysis of Maslov [17], which analysed the JET-C dataset in detail. The regression analysis in [17] reports $\tau_{\mathrm{E,th}} \propto A^{0.2}$ for a JET-C dataset of $\sim$ 1000 samples, which includes Hydrogen (H), Deuterium (D), Tritium (T) and DT plasmas at all densities.

JT-60U found that a positive isotope dependence of the thermal energy confinement time arises from the core in type I ELMy H-modes and the pedestal structure has no direct dependence on the isotope mass [3, 4, 5]. Studies on ASDEX-Upgrade have reported that roughly a factor of 2 higher heating power is required to match the pedestal pressure in H and D [9].

Recent isotope experiments in H and D plasmas in JET with the ITER-like Wall (JET-ILW) showed a doubling of the power threshold for type III/type I ELMs from D to H [1]. In type I ELMy H-mode plasmas a positive scaling of $\tau_{\mathrm{E,th}}$ with the isotope mass was observed: $\tau_{\mathrm{E,th}} \propto A^{0.4}$ [1, 18, 19]. The gradient length (R/L_T, where R is the major radius, $L_T = T/\nabla T$ and T is the temperature) of core temperature profiles was similar

in H and D, despite large variations in the heat flux [1, 18, 19]. This suggests that the isotope effect may originate in the pedestal in conditions where ions and electrons are collisionally coupled and electron and/or ion transport are stiff [1]. At the same input power and fuelling gas rate, the pedestal pressure is typically reduced in H compared to D, primarily due to lower pedestal density in H. Note that, similar gas fuelling rate in H and D does not necessarily lead to similar main chamber neutral pressure with the two isotopes, but due to lack of measurements any difference could not be quantified. In H and D type I ELMy H-modes at the same pedestal pressure, which requires roughly double input power in H than in D at same gas injection, the low pedestal density in H is compensated by higher temperature. These observations suggest that understanding the reduced particle transport with increasing isotope mass is crucial to explain the isotope effect in the JET-ILW pedestal.

In order to understand the isotope dependence of plasma confinement, comparative experiments aim to observe differences under the same experimental conditions, when an isotope is substituted for another. This task is extremely difficult due to the number of parameters affecting the isotope dependence, and the measurability and controllability of these parameters [19]. For example, NBI heating with different species could lead to differences in particle and heat deposition. Gas fuelling may affect edge and divertor conditions differently, because the velocity, thus the mean free path of the neutrals is mass dependent. In order to distinguish between the direct and indirect effects introduced by the variation in isotope mass, in our study, the isotope dependence of the JET-ILW pedestals has been investigated by taking a database approach on the one hand, where a large number of type I ELMy H-modes are compared under parameter variations such as gas rate and input power. On the other hand, a representative hydrogen and deuterium pair have also been selected for detailed analysis. The paper focuses on the isotopic dependence of the type I ELMy H-mode pedestal. In particular, the pedestal structure, edge transport and the isotope effect on linear MHD stability are analysed in a series of JET-ILW H and D type I ELMy H-mode plasmas.

The paper is organised as follows. Section 2 describes the data set of JET-ILW H and D type I ELMy H-modes used in this work with the characterisation of the pedestal structure. ELM energy and particle losses are compared between H and D in section 3 using Thomson scattering measurements, the stored energy signal from EFIT magnetic equilibrium reconstructions, and interferometry for particle losses. Investigation of the edge plasma and the scrape-off layer using interpretative EDGE2D-EIRENE simulations to examine the role of neutral penetration and edge transport is presented in section 4. In section 5, the isotope dependence of the pedestal stability is examined with the HELENA fixed boundary equilibrium and ELITE linear ideal MHD stability codes. A summary and conclusions are presented in section 6.

2. Pedestal structure in JET-ILW H and D type I ELMy H-modes

In the present paper JET-ILW type I ELMy H-modes at low plasma triangularity ($\delta \approx 0.2$) with mostly NBI heating are analysed. The clear separation between type I and type III ELMy H-modes in these plasmas has already been discussed in [1]. The dataset includes power ($P_{\mathrm{NBI}} = 3{-}16$ MW) and gas scans at two different plasma current and magnetic field combinations (1.0 MA/1.0 T with $q_{95} = 3.0$ and 1.4 MA/1.7 T with $q_{95} = 3.7$). At 1.4 MA/1.7 T, β_N varies between 1.4 and 2.8 in D, but only between 1.3 and 1.7 in H due to the limited power delivered by the hydrogen NBI (10 MW). 1.0 MA/1.0 T plasmas are also explored in order to extend the range of β_N in H: at 1.0 MA/1.0 T, β_N varies between 1.7 and 2.7 in D and between 1.4 and 2.2 in H. The discharges analysed are steady over $> 7 - 8 \times \tau_{\mathrm{E,th}}$ or longer (the selected time windows are longer than 1.5 s in all cases, typically $2 - 3$ s). Hereinafter, the H_2/D_2 gas rates will be referred to as "low" $= 3 - 4.5 \cdot 10^{21}$ e/s, "medium" $= 8 - 10 \cdot 10^{21}$ e/s and "high" $= 16 - 18 \cdot 10^{21}$ e/s. NBI was operated with the ion species of the plasma (H-NBI in H and D-NBI in D plasmas). The plasma purity was higher than 97 % both in H and D.

The majority of the dataset is in the so-called C/C divertor configuration, where both divertor strike points are close to the pumping duct. One power scan (1.4 MA/1.7 T, at low gas rate) is in the so-called V/H configuration, where the inner strike point is on the vertical target and outer strike point is on the horizontal target. Due to a 2-3 fold increase in sub-divertor neutral pressure, and thus improved cryo-pumping, operation in C/C configuration leads to a $15 - 20$ % decrease in $n_{\mathrm{e,PED}}$ and a similar increase in $T_{\mathrm{e,PED}}$ at similar $p_{\mathrm{e,PED}}$ values than in V/H configuration in D H-modes [20].

The pedestal structure in the D plasmas of the 1.4 MA/1.7 T dataset has already been characterised elsewhere [20, 21], but here some of those findings are recalled for comparison with the H plasmas. First, the ELM frequency (f_{ELM}) as a function of the power crossing the separatrix (P_{sep}) is shown in figure 1 to demonstrate the type I nature of the ELMs, i.e. increasing f_{ELM} with P_{sep}. P_{sep} is defined as follows,

$$P_{\mathrm{sep}} = P_{\mathrm{loss}} - P_{\mathrm{rad,bulk}} = P_{\mathrm{abs}} - \langle \mathrm{d}W/\mathrm{d}t \rangle - P_{\mathrm{rad,bulk}} \ , \tag{1}$$

where P_{abs} is the total absorbed power given by the sum of the Ohmic power, the absorbed neutral beam power (accounting for shine through) and absorbed ion cyclotron heating power (where applicable). $P_{\mathrm{rad,bulk}}$ is the total radiated power inside the separatrix as estimated by a weighted sum of representative bolometer channels, P_{loss} is the loss power given by $P_{\mathrm{loss}} = P_{\mathrm{abs}} - \langle \mathrm{d}W/\mathrm{d}t \rangle$. $\langle \mathrm{d}W/\mathrm{d}t \rangle$ is the rate of change of the total stored energy averaged over a timescale longer than the ELM period. This is negligible in the steady phases of the discharges that are used for the analysis here, but it is show in eq. (1) for completeness.

f_{ELM} is typically higher in H than in D at given gas rate and input power, except for the one medium gas pulse in H at 1.4 MA/1.7 T. Note that NBI heating was limited to 10 MW in H, thus in some of the H plasmas at 1.4 MA/1.7 T (symbols with a black dot inside in figure 1), 2-5 MW ion cyclotron resonance heating (ICRH: 51 MHz, H

majority, 2nd harmonic) was added to the heating mix to reach type I ELMy H-modes, which is expected to lead to an increase in f_{ELM} compared to NBI only plasmas [22]. All other plasmas were NBI heated only.

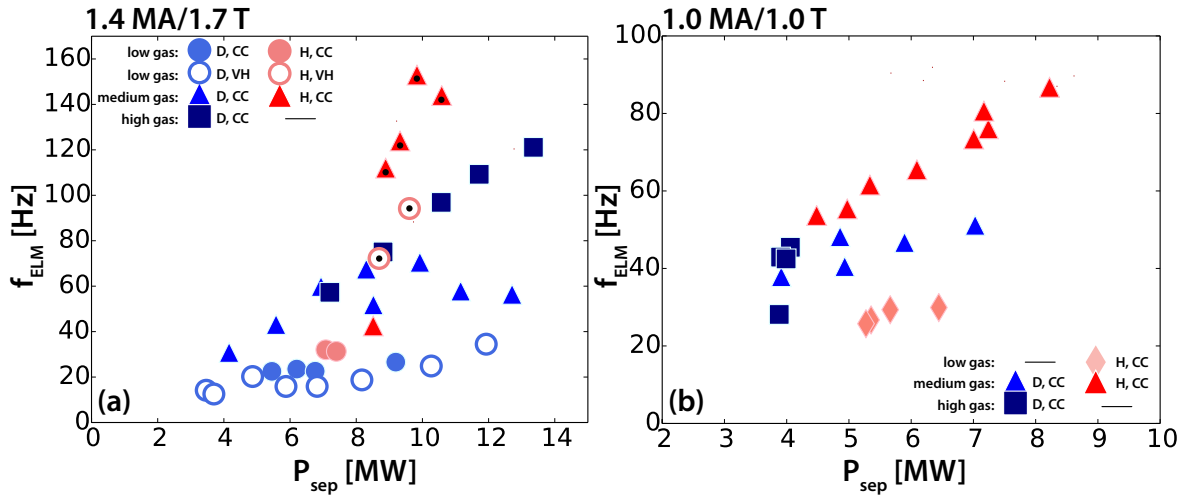

Figure 1. ELM frequency as a function of net power crossing the separatrix for the (a) 1.4 MA/1.7 T and the (b) 1.0 MA/1.0 T dataset. Symbols with a black dot inside represent NBI+ICRH heated pulses.

The pedestal structure analysis is carried out for the pre-ELM phase (namely the last 20 % of the ELM cycle) and is based on the mtanh [23] fitted electron density (n_e) and temperature (T_e) profiles as measured by Thomson scattering (TS) [24]. The kinetic profiles, collected from a steady time window of the discharge, are ELM-synchronised to improve signal statistics [25, 26]. The width and height of the pedestal electron density and temperature are taken directly from the mtanh fit. The error bars on the pedestal structure parameters are defined as the standard deviation of the parameter estimates of the mtanh fit.

2.1. Pedestal height

In what follows we show the main differences in the pedestal structure between H and D pulses. Figure 2 shows the electron pedestal pressure ($p_{e,PED}$ [Pa] $= 1.602 \times n_{e,PED}/10^{19}$ [m^{-3}]$\times T_{e,PED}$ [eV], where 1.602 originates from the elementary charge as T_e is measured in eV) as a function of P_{sep}. Both at 1.0 MA/1.0 T and 1.4 MA/1.7 T, $p_{\mathrm{e,PED}}$ decreases with increasing gas rate at a given P_{sep}, isotope and divertor configuration. In general, $p_{\mathrm{e,PED}}$ is higher in D than in H at a given P_{sep}, but the difference is more pronounced at low gas rate.

The edge n_e-T_e diagram in figure 3 shows that pedestals at the same $p_{\mathrm{e,PED}}$ (typically obtained with more heating power in H than in D) have lower density, but higher temperature in H compared to D. In other words, by varying input power and/or gas rate it was not possible to simultaneously match n_e and T_e in H and D, as for example in JT-60U experiments [3, 4, 5]. It is also visible in figure 3a, that $n_{\mathrm{e,PED}}$ is slightly

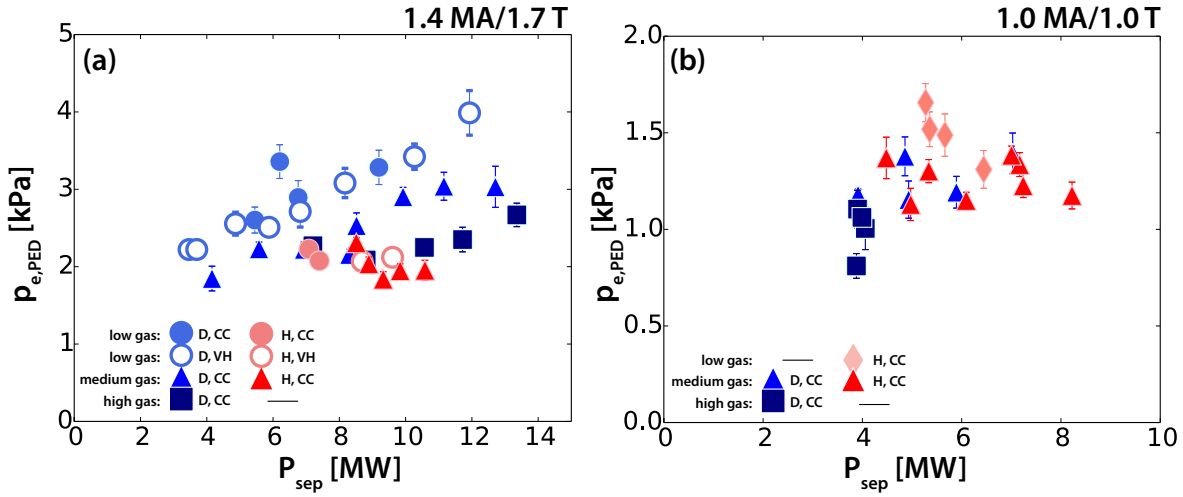

Figure 2. The electron pressure at the pedestal top as a function of net power crossing the separatrix for the (a) 1.4 MA/1.7 T and the (b) 1.0 MA/1.0 T dataset.

higher in V/H configuration than in C/C at similar $p_{e,PED}$, but it is important to note that $n_{e,PED}$ is lower in H than in D at given $p_{e,PED}$ and divertor configuration.

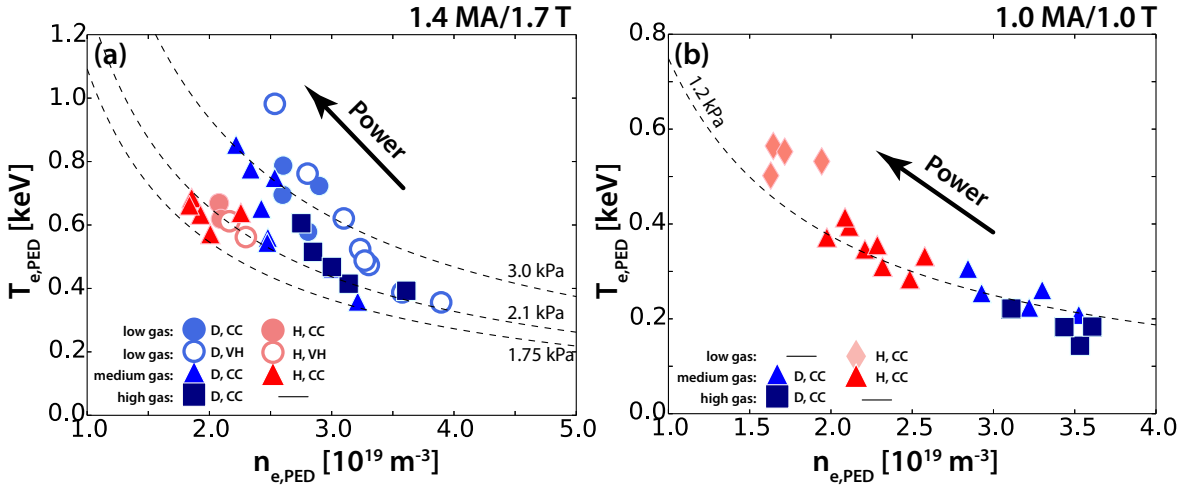

Figure 3. $n_{e,PED}$-$T_{e,PED}$ diagram for the (a) 1.4 MA/1.7 T and the (b) 1.0 MA/1.0 T dataset. The dashed black lines are isobars at a pressure level indicated in the figure.

At 1.0 MA/1.0 T and medium gas rate $p_{e,PED}$ is comparable in H than in D as shown on both figure 2b and 3b, but the total thermal stored energy is still higher in D. The gradient lengths in the core are very similar and any difference in the temperature gradient length arises at $\rho_{TOR} > 0.8$, as shown in figure 4. This is a representative example, where the electron kinetic profiles on a log scale (for comparison of the core gradient lengths) are shown for a pair of H and D pulses at the same P_{sep}. Therefore, for the 1.0 MA/1.0 T medium gas rate dataset as well, the difference in thermal energy confinement between H and D is emerging at the edge.

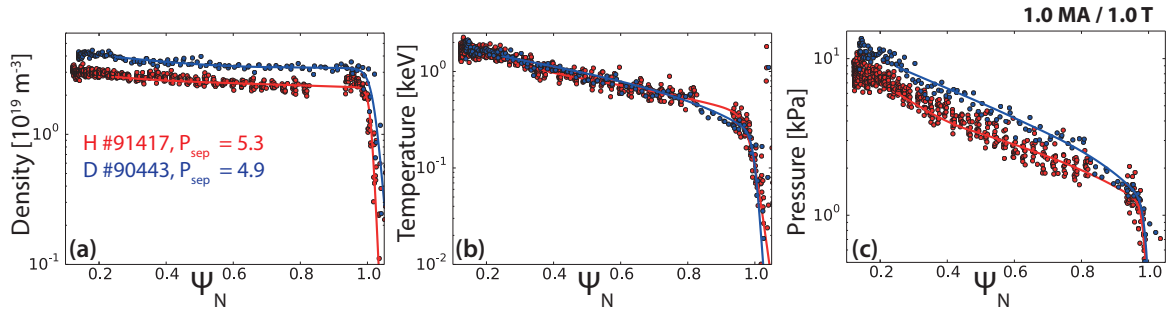

Figure 4. pre-ELM (80-100 % of the ELM cycle) electron kinetic profiles from TS for a pair of H (#91417, in red) and D (#90443, in blue) pulses at 1.0 MA/1.0 T at the same $P_{\rm sep}$ as a representative example. (a) Electron density, (b) electron temperature and (c) electron pressure are shown on a log scale to compare the gradient lengths in the core. Profiles are radially shifted to have $T_{\rm e,sep} = 100$ eV.

The ion temperature (T_i) is similar to T_e at the pedestal top within the measurement uncertainties of the edge Charge Exchange Recombination Spectroscopy (CXRS) system. Discharges with good T_i data in the pedestal gradient region confirm $T_e \approx T_i$, although T_i at the separatrix cannot be resolved. The line-averaged $Z_{\rm eff}$ in the 1.4 MA/1.7 T dataset varies between 1.1 and 1.5 for D and between 1.2 and 1.8 for H. For the 1.0 MA/1.0 T dataset it varies between 1.2 and 1.4 for D and between 1.1 and 1.4 for H. Assuming Be as single impurity and $T_e = T_i$, the ion dilution leads to at most 10 % difference between the total pressure (calculated as $p = p_e + p_i$) and $2 \times p_e$, thus the conclusions drawn from the analysis of the electron pressure also apply to the total pressure.

3. ELM energy and particle losses

In this section ELM energy losses are investigated to establish the the power balance of the pedestal in terms of radiation, ELM losses and inter-ELM transport. As ELMs are dominated by particle losses in the investigated discharges, ELM particle losses are separately discussed in section 3.2.

3.1. Power balance and ELM energy losses

Compared to eq. (1), $P_{\rm sep}$ in the power balance equation here is separated into inter-ELM and ELM components and $\langle {\rm d}W/{\rm d}t \rangle$ is omitted as only the steady phases of the discharges are examined, where the rate of change of stored energy on time scales longer than the ELM cycle is negligible:

$$P_{\rm sep} = P_{\rm inter-ELM} + P_{\rm ELM} = P_{\rm loss} - P_{\rm rad,bulk} \tag{2}$$

The ELM energy loss ($\Delta W_{\rm ELM}$) - which gives $P_{\rm ELM} = \Delta W_{\rm ELM} \times f_{\rm ELM}$ - has been evaluated from two independent measurements: a) the stored energy from EFIT equilibrium reconstruction ($\Delta W_{\rm MHD}$) and b) Thomson scattering electron kinetic profile

measurements (ΔW_{TS}). ΔW_{MHD} is estimated by the difference between the maximum and the minimum of the W_{MHD} signal in the vicinity of the ELM crash as illustrated by the red arrow in figure 5. ΔW_{MHD} is evaluated for all ELMs individually in the steady phase of the discharge. The ELM energy losses are then averaged and their standard deviation provides a measure for the scatter in ΔW_{MHD}, which will be represented with error bars.

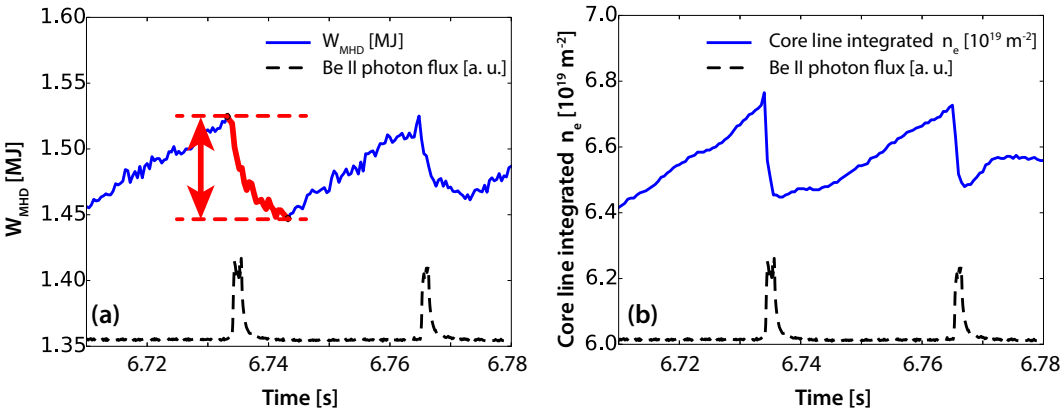

Figure 5. (a) Stored energy signal (W_{MHD}) from EFIT equilibrium reconstruction and (b) the line-integrated density from the core interferometry channel during an ELM crash in H pulse #91554. The inner divertor BeII (λ = 527 nm) photon flux (dashed black line) is used as an ELM marker in both figures.

ΔW_{TS} is evaluated by applying the method explained in [27]: In the steady phase of the pulse, the pre- and post-ELM TS profiles are fitted using the ELM synchronisation technique to compensate for the low time resolution (20 Hz) of the TS diagnostic. The post-ELM profile fit represents roughly the 5-15 % interval of the ELM period. TS measurements taken during the ELM crash are excluded as the profiles in this interval are often dominated by the particular dynamics of each ELM crash. Typically 2 or 3 TS measurements following the ELM crash are selected. An example is shown in figure 6, where pre-ELM (80-97 %) and post-ELM (5-15 %) electron density (figure 6a) and temperature (figure 6b) TS profiles can be seen for D discharge #84796. The ELM energy loss is calculated from the difference between the pre- and post-ELM TS profiles volume integrated in the region $\Psi_N = [0.5, 1.0]$:

$$\Delta W_{\mathrm{TS}} = \frac{3}{2} k \left(\int_V n_{\text{pre-ELM}} T_{\text{pre-ELM}} \mathrm{d}V - \int_V n_{\text{post-ELM}} T_{\text{post-ELM}} \mathrm{d}V \right), \qquad (3)$$

where k is the Boltzmann constant. $T_i = T_e$ is assumed and line-averaged Z_{eff} measurements (assuming Be as single impurity) are taken into account to evaluate the total ELM energy loss. The effect of ELMs on the kinetic profiles is negligible inside the mid-radius (see figure 6 for example), thus the TS profiles are integrated only from $\Psi_N = 0.5$. Due to ELM synchronisation, ΔW_{TS} is already an average over the steady phase of the discharge. The uncertainty of ΔW_{TS} is estimated from the errors of the pedestal top values of the mtanh fit.

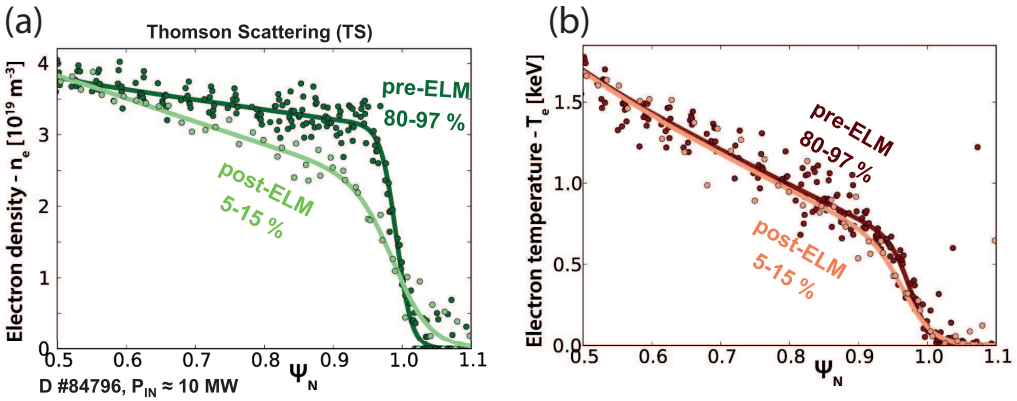

Figure 6. The mtanh fitted pre-ELM (80-97 %) and post-ELM (5-15 %) density (a) and temperature (b) profiles of D pulse #84796.

A comparison of ELM losses evaluated from ΔW_{MHD} and ΔW_{TS} for selected pulses of the isotope dataset is shown in figure 7. The ELM losses evaluated by the two measurements are broadly consistent, especially in controlled parameter scans, but differences between individual discharges can be as high as a factor of 2 due to the intrinsic uncertainties of this analysis. These include uncertainties in ΔW_{MHD} due to slow data acquisition of the magnetic diagnostics, screening of the vacuum vessel and other conducting structures and uncertainties in ΔW_{TS} due to uncertainties in the TS measurement and errors introduced by ELM-synchronisation and regularisation of the profile by the mtanh fit. Due to these difficulties with the measurements, ELM energy losses can only be evaluated below $f_{\mathrm{ELM}} \approx 50 - 60$ Hz, which is a typical condition for the low gas rate pulses in the isotope dataset. Thus, figure 7 shows a subset of JET-ILW H and D type I ELMy H-modes, where the ELM frequency satisfies this condition.

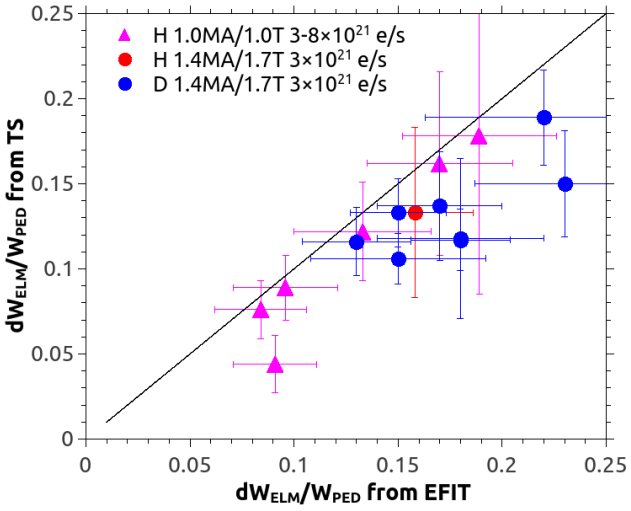

Figure 7. Comparison of ELM losses evaluated from W_{MHD} and TS profiles on a subset of JET-ILW H and D type I ELMy H-modes.

The power balance analysis is presented here for selected discharges with plasma current $I_p = 1.4$ MA, toroidal magnetic field $B_t = 1.7$ T, fuelling gas rate $\Gamma_e = 3 - 4 \times 10^{21}$ e/s and NBI heating. The ELM-averaged pedestal kinetic profiles of the selected pulses are shown in figure 8. It shows the pedestal profiles of electron density, temperature and pressure for a H reference discharge in red (#91554) and two deuterium plasmas with similar thermal stored energy (in blue, #84793) and input power (in black, #84796) of the hydrogen counterpart. The main parameters of these 3 discharges can be seen in table 1.

Shot	Γ_e [10^{21} e/s]	P_{NBI} [MW]	P_{loss} [MW]	W_{th} [MJ]	n_e [10^{19} m^{-3}]	n_e/n_{GW}	NBI part. src. [10^{21} s^{-1}]	edge src. [10^{21} s^{-1}]	f_{ELM} [Hz]
#84793 D	2.8	4.4	4.6	1.2	3.7	0.76	0.46	6.4	14.2
#84796 D	2.8	10.6	10.4	1.9	3.5	0.77	1.1	-	18.7
#91554 H	4	10.0	9.4	1.1	2.5	0.52	1.7	12.5	31.3

Table 1. Main parameters of the 1.4 MA/1.7 T, $\delta = 0.2$, H and D plasmas selected for comparison. n_e is the line-integrated core density from interferometry, n_e/n_{GW} is the Greenwald fraction, "NBI part. sec." is the particle source from NBI fueling and "edge src." is the ionisation source as estimated with interpretative EDGE2D-EIRENE simulations (only for #84793 and #91554, see section 4 for more details). Note that $P_{loss} = P_{NBI}^{abs} + P_{Ohmic} - \langle dW/dt \rangle$ is evaluated using the absorbed neutral beam power (accounting for shine through), while P_{NBI} is the injected power.

The comparison of H and D plasmas at similar stored energy (#91554 and #84793) shows that roughly two times higher heating power is needed in H to match the stored energy of the D counterpart. In this comparison the pedestal pressure is also similar and the lower density in H is compensated by the higher temperature as shown in figure 8. When the heating power is similar in H and D (#91554 and #84796), the pedestal temperature is similar too, but the pedestal density is significantly lower in H.

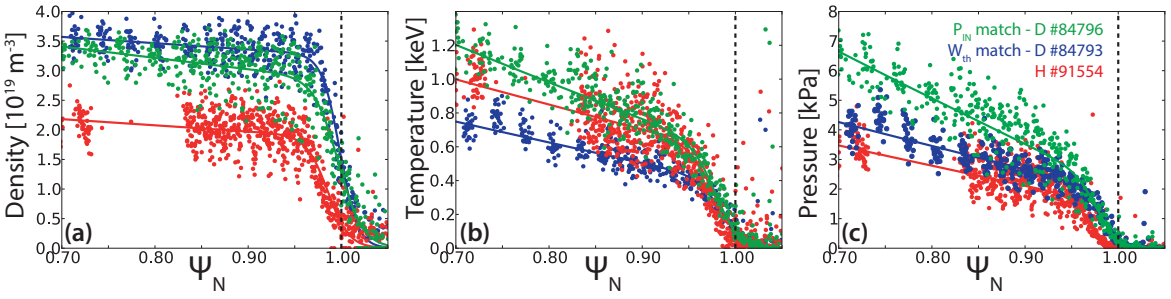

Figure 8. ELM-averaged (0-100 % of the ELM cycle) electron kinetic profiles from TS of the pedestal for the hydrogen reference discharge (#91554) and the two deuterium plasmas with similar thermal stored energy (#84793) and similar input power (#84796) to that of the hydrogen counterpart. (a) Electron density (b) electron temperature (c) electron pressure. These profiles are radially shifted to have $T_{e,sep} = 100$ eV.

The result of the power balance analysis for the 3 discharges characterised above is summarised in table 2. The comparison of H and D plasmas at similar stored energy (#91554 and #84793) shows that roughly double inter-ELM separatrix loss power is required in H than in D to maintain the same pedestal top pressure. This is in agreement with observations of ASDEX-Upgrade H-mode plasmas [9]. When the heating power is similar in H and D (#91554 and #84796), inter-ELM separatrix loss powers are also similar.

Shot	$P_{\rm loss}$ [MW]	$P_{\rm rad}$ [MW]	f_{ELM} [Hz]	ΔW_{ELM} [kJ]	P_{ELM} [MW]	P_{sep} inter-ELM [MW]	$p_{e,PED}$ [kPa]	$\nu_{e,PED}$
#84793 D	4.6	1.1	14.2	76	1.1	2.4	2.2	1.7
#84796 D	10.4	2.2	18.7	126	2.4	5.8	3.1	0.7
#91554 H	9.4	2.0	31.3	74	2.3	5.1	2.1	0.5

Table 2. Power balance analysis for the three discharges at 1.4 MA/1.7 T and low gas rate introduced in table 1.

3.2. ELM particle losses

We now analyse how ELMs affect the particle and energy channels, respectively. Figure 6a and b show the pre-ELM (80-97 %) and post-ELM (5-15 %) TS profiles for discharge #84796. In this example, the ELMs primarily affect the density, not so much the temperature profiles. This behaviour is general in the analysed isotope dataset and applies to both H and D type I ELMy H-modes as indicated by figure 9, where the relative drop of the pedestal top density and temperature is shown for H and D plasmas at 1.4 MA/1.7 T (circles) and 1.0 MA/1.0 T (triangles). A comparison of the fuelling sources in representative plasmas (from EDGE2D-EIRENE simulations, see section 4) and an order of magnitude estimate for the ELM particle losses utilising the TS measurement suggests that ELMs could be responsible for $\sim 20-30$ % of the total particle losses. In view of this, ELM particle losses are investigated here in detail.

ELM energy losses primarily due to the loss of particles have also been observed in low triangularity JET-C experiments, where $f_{\rm ELM}$ was increased by increasing the fuelling gas rate [28, 29]. At low $f_{\rm ELM}$, ELM energy losses (relative to the total stored energy) and the relative temperature drop were high, with smaller relative density drop. With increasing $f_{\rm ELM}$, the ELM energy losses decreased, primarily due to the reduction of the relative temperature drop and no change in the relative density drop. Hence, the high frequency ELMs mainly affected the density pedestal, similarly to the ELMs observed in the JET-ILW isotope experiments described here.

As it was shown in section 2, the pedestal density in D is significantly higher than in H at similar $P_{\rm sep}$ in the JET-ILW isotope dataset. However, it has also been shown that the ELM frequency is typically higher in H in these conditions. Figure 10a shows the pedestal top density as a function of $f_{\rm ELM}$ in H and D for the low gas 1.4 MA/1.7 T and the medium gas 1.0 MA/1.0 T datasets. In these low triangularity plasmas ($\delta \approx 0.2$),

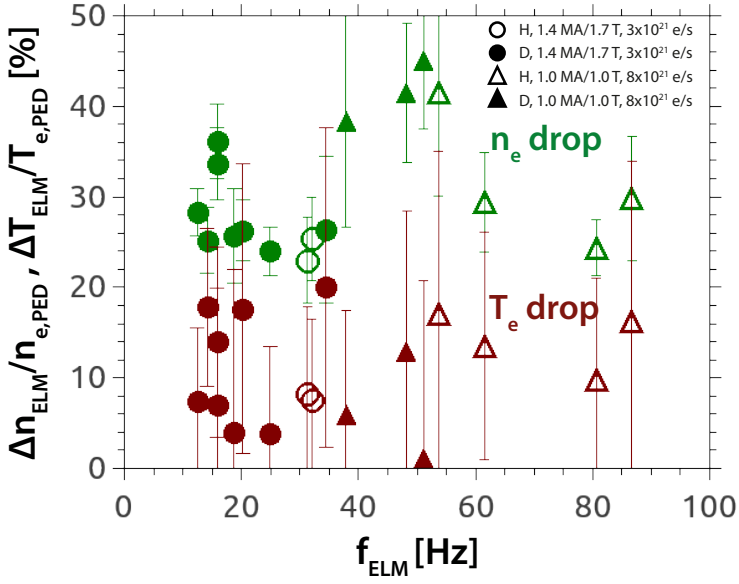

Figure 9. The relative drop of the pedestal top density and temperature at the ELM crash as a function of the ELM frequency for H (open symbols) and D (full symbols) plasmas at 1.4 MA/1.7 T low gas rate (circles) and 1.0 MA/1.0 T medium gas rate (triangles).

$n_{\mathrm{e,PED}}$ decreases as f_{ELM} is increased by increasing input power. H and D pedestals at similar f_{ELM} (obtained at different P_{sep}) have comparable pedestal densities, as highlighted by the black dashed circles in figure 10a.

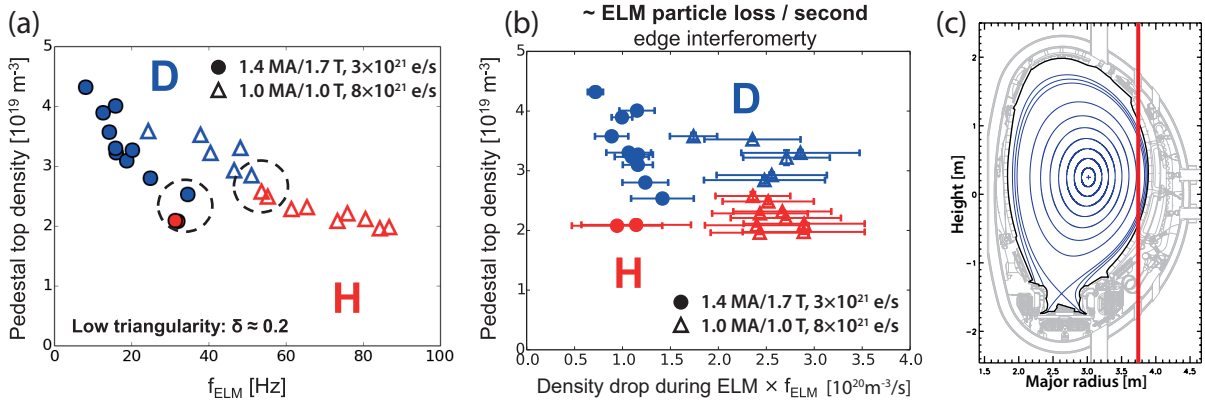

Figure 10. (a) $n_{\mathrm{e,PED}}$ as a function of f_{ELM} in low $\delta(= 0.2)$ H (red) and D (blue) plasmas at 1.4 MA/1.7 T (full circles) and 1.0 MA/1.0 T (open triangles). H and D pedestals at similar f_{ELM} (but different P_{sep}) have comparable pedestal densities as highlighted by the black dashed circles. (b) $n_{\mathrm{e,PED}}$ as a function of average drop in edge interferometer signal during ELMs per second. The error bars represent the statistical variation of the ELM particle loss throughout the steady phase of the discharge. (c) The line-of-sight of the edge interferometry channel (in red) used for the ELM particle loss analysis in a poloidal cross-section of JET-ILW.

In order to shed light on the cause of the correlation between f_{ELM} and $n_{\mathrm{e,PED}}$ in the H and D isotope database, the ELM particle losses are investigated. High resolution profiles measurements were not available for the plasmas in the analysed dataset. The TS system has slow time resolution (20 Hz) and the reflectometry is not available below $B_t = 2$ T. Therefore, the edge interferometer [30] was utilised to estimate the particle loss in an ELM crash. It provides a line integrated density measurement at the plasma edge, as shown in figure 10c. The drop in the line-averaged interferometer signal during the ELM crash times the ELM frequency is taken as proxy for the total ELM induced particle loss ($f_{\mathrm{ELM}} \times \Delta n_{\mathrm{ELM}}$). Figure 10b shows the pedestal density as a function of this proxy for ELM particle losses. At a given configuration (I_p/B_t), particle losses in H and D plasmas are similar within the uncertainties. It is important to note, that the interferometry data can only be used for comparing ELM particle losses between the 1.4 MA/1.7 T H and D plasmas with the caveat that due to the differences in divertor geometry, the interferometer line-of-sight (LOS) between the H and D plasmas are different leading to a systematic bias.

3.3. Discussion on the role of ELM particle losses in setting the pre-ELM pedestal structure

Although the absolute comparison of the ELM particle losses between the H and D pulses is challenging, the 1.4 MA/1.7 T Deuterium power scan (where the divertor geometry and plasma shape, thus the interferometer LOS were fixed) exhibits a reduction in pedestal density with the increase of ELM particle losses as can be seen in figure 10b. This implies that the higher ELM particle losses may contribute to lower pedestal density in some circumstances. It is expected that pedestal MHD stability determines the maximum achievable pressure, but not the ratio of the pedestal density and temperature. Higher ELM particle losses may set a lower density in the inter-ELM phase. Considering a simple diffusive inter-ELM transport model, lower density would lead to reduced heat transport. A reduction in the inter-ELM heat transport would accelerate the recovery of the pedestal temperature and thus ELMs may be triggered at relatively higher temperature, but lower density. Further experiments (such as power scans in different isotopes with high time resolution density profile measurements) are required to conclusively quantify the role of ELM particle losses in explaining the differences between pedestals observed in H and D.

4. Interpretative EDGE2D-EIRENE simulations

In the present section, an edge transport analysis comparing H and D type I ELMy H-modes with EDGE2D-EIRENE [31, 32, 33] is discussed. EDGE2D is a 2D fluid code with realistic geometry of the SOL and divertor region, which is coupled to EIRENE, a Monte Carlo code used to calculate the neutral particle distribution. These simulations help to understand how transport and neutral penetration affect the pedestal performance

when the isotope mass is changed. Furthermore, these allow us to study the isotope dependence of the pedestal through changes in divertor conditions.

4.1. Edge plasma properties in H and D type I ELMy H-modes

EDGE2D-EIRENE is used here to investigate neutral penetration and plasma transport in H and D type I ELMy H-modes. A pair of type I ELMy H-modes at low gas rate (#91554 and #84793) with similar stored energy were selected (see table 1). Note that the input power is doubled in H compared to D to reach similar stored energy and pedestal pressure, and the H pulse has lower $n_{\mathrm{e,PED}}$ and higher $T_{\mathrm{e,PED}}$ than the D pulse (see figure 8).

EDGE2D-EIRENE is run in interpretative mode, where the perpendicular transport coefficient of electron particle diffusion $D_\perp$ ($\Gamma_e = D_\perp \nabla n_e$), electron and ion heat transport $\chi_{e,i}$ ($q_{e,i} = -n_{e,i}\chi_{e,i}\nabla T_{e,i}$) and the pump albedo were iterated until the solution fitted the measured upstream n_e and T_e profiles (measured by TS) and the outer target heat deposition profile (measured by IR-camera). Some technical details on the pump albedo can be found in Appendix A. χ_e and χ_i were assumed to be the same, due to lack of constraints. χ in the SOL was set such that the heat deposition profile at the outer divertor target matched the IR camera measurements. The aim here was to approximately match the width of the heat deposition profile in order to constrain the width of the SOL, which potentially affects the value of the separatrix temperature through changes in heat flux density arriving to the SOL.

The grid for EDGE2D relies on EFIT equilibrium reconstruction. The simulation domain extends to $\sim 10-15$ cm inside the separatrix to the core plasma. The NBI and gas fuelling was set in accordance with the experiment. The input power in EDGE2D was set to the power crossing the separatrix inter-ELM, i.e. the ELM power loss (P_{ELM}) was excluded. The ELM crash was not simulated and it was assumed that P_{ELM} does not contribute to the power balance in the SOL, which sets the separatrix temperature inter-ELM. For simplicity, both the H (#91554) and the D (#84793) cases were simulated in the corner-corner (C/C) divertor target configuration, albeit discharge #84793 was in vertical-horizontal (V/H) divertor target configuration in the experiment. The pedestal density is approximately 20 % higher in V/H than in C/C configuration, but the difference in $n_{\mathrm{e,PED}}$ between the H and D pulses (#91554 and #84793, see figure 4) investigated in this section is much higher - approximately 50 % - than what could be attributed to the different divertor configurations. More details on the divertor configuration and on the grid definition is shown in Appendix B and Appendix C, respectively.

Figure 11 shows the "inter-ELM" (40-80 % of the ELM cycle) n_e and T_e profiles measured by TS (in grey) and the profiles of the EDGE2D-EIRENE solutions (in red for H and blue for D). The "inter-ELM" outer target heat flux profiles are evaluated

by averaging the profiles from the IR camera in the 40-80 % part of the ELM cycle‡ and are compared with the EDGE2D simulations in figure 12. The implications on the separatrix temperatures indicated in figure 11 will be discussed in section 4.2.

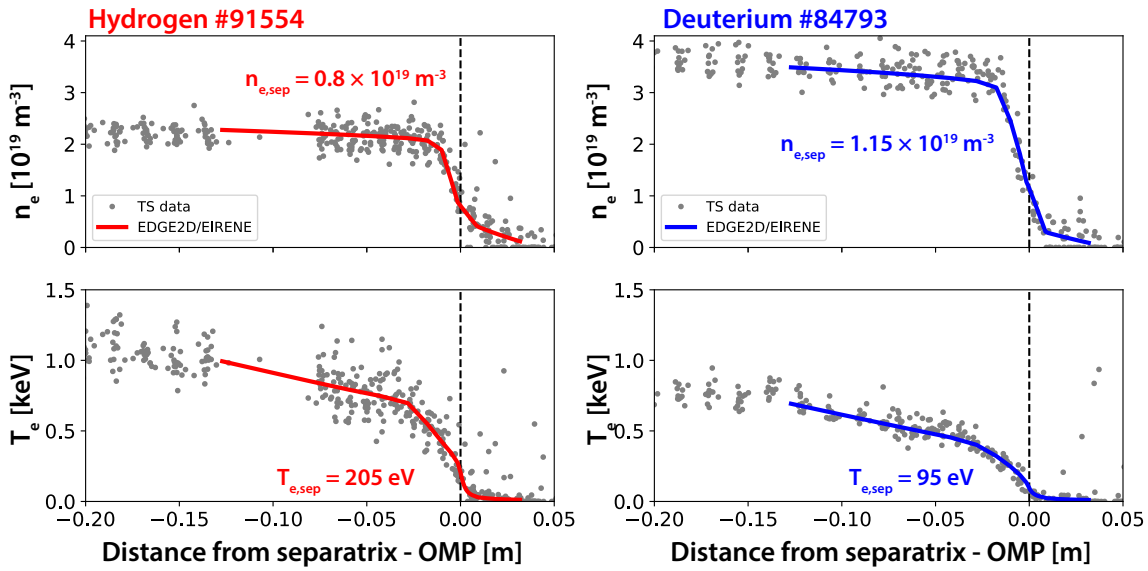

Figure 11. Inter-ELM TS profiles (40-80 % of the ELM cycle) for n_e and T_e (in grey) in the steady phase of the H (#91554: 5.7-8.2 s) and D (#84793: 5.0-6.3 s) discharges. The resulting upstream n_e and T_e profiles of the interpretative EDGE2D-EIRENE simulations for the H pulse (#91554) in red and for the D pulse (#84793) in blue.

Figure 13 shows the anomalous transport coefficients used in the simulations to match the experimental upstream and divertor target profiles. The anomalous heat transport coefficients inside of the pedestal are higher in H than in D, but are comparable in the edge transport barrier (ETB). $D_\perp$ is higher in H than in D everywhere inside the separatrix. This implies that larger particle transport in H than in D could be responsible for the lower $n_{\mathrm{e,PED}}$ in H. The structure in the $D_\perp$ and $\chi_{e,i}$ profiles in the ETB (see figure 13) were needed in EDGE2D-EIRENE to match the TS data, but it is important to note that $T_{\mathrm{e,sep}}$ is not sensitive to these fine details in the shape of the perpendicular transport coefficients. $\chi_{e,i}$ outside the separatrix is constrained by the outer target IR heat deposition profile, but there is insufficient information from IR to distinguish between H and D. Similarly, n_e in the SOL from TS is too uncertain to constrain $D_\perp$, which was therefore imposed to be the same in H and D.

The effect of change in mean free path of neutrals between H and D in the EDGE2D-EIRENE simulations is investigated with a test where all input parameters (transport coefficients, pump albedo, input power, gas fuelling, etc.) are kept fixed to the values

‡ The time evolution of heat deposition reconstructed from IR measurements can be very uncertain in the vicinity of the ELM crash due to the transient heat flux arriving to the target. Thus, the 40-80 % interval was chosen to represent the inter-ELM parameters and exclude any artefacts in the heat deposition profiles. TS data are also filtered for the 40-80 % part of the ELM cycle for consistency.

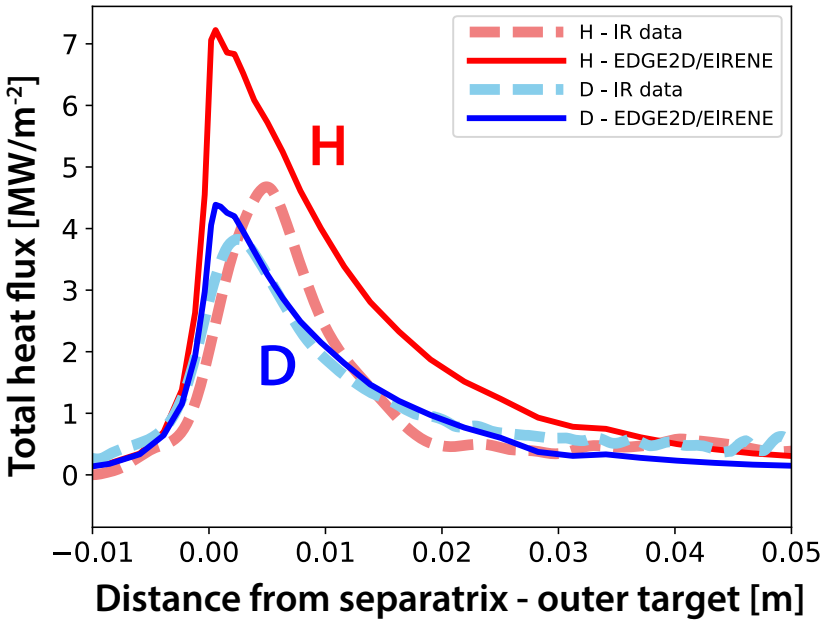

Figure 12. Inter-ELM (40-80 % of the ELM cycle) outer target heat deposition profiles as evaluated from IR camera measurements in the steady phase of the H (#91554: 5.7-8.2 s) and D (#84793: 5.0-6.3 s) discharges with dashed lines. Outer divertor target heat deposition profiles from EDGE2D-EIRENE with solid lines for H (red #91554) and D (blue #84793).

of the interpretative runs for the D pulse #84793, but the isotope mass is changed from D to H. The input parameters of the interpretative simulation for the D case (#84793) were taken. The results of the change from D to H for otherwise fixed conditions is only a ~ 10 % increase in the pedestal top density and a slight decrease in the temperature, as shown in figure 14. The change in upstream profiles is much smaller and even opposite to experimental observations (see figure 8). Therefore, we conclude from these studies that the change in neutral penetration when the isotope mass is changed does not explain the observed lower density in H pedestals and therefore changes in transport and stability must also play a role.

4.2. Separatrix temperature in H and D type I ELMy H-modes

The interpretative EDGE2D-EIRENE simulations with constrained upstream and target profiles yield a more accurate value for the electron separatrix temperature than the widely used $T_{\mathrm{e,sep}} \approx 100$ eV assumption [37, 38, 39, 40, 41, 42, 43] obtained by the 2-point model [44, 45]. The knowledge of $T_{e,sep}$ is required to constrain the separatrix position for the radial alignment of the measured kinetic profiles. The position of the separatrix from magnetic constrained EFIT is uncertain ($\sim 1-2$ cm) and typically implies unphysical separatrix temperatures ($\ll 100$ eV) due to the uncertainties in the magnetic equilibrium reconstruction. An estimate for $T_{e,sep}$ can be obtained by taking into account the parallel heat conduction and pressure and power balance in the scrape-

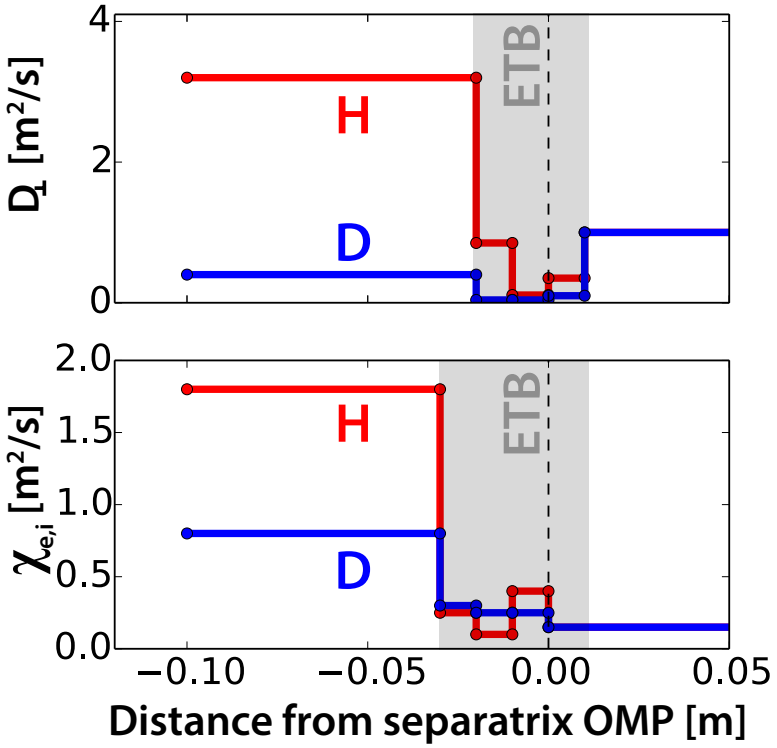

Figure 13. Electron particle diffusion ($D_\perp$) and electron and ion heat transport ($\chi_e = \chi_i = \chi_{e,i}$) coefficients of the EDGE2D-EIRENE simulations for the inter-ELM phase (40-80 %) of the H (red #91554) and D (blue #84793) discharges. The edge transport barrier (ETB) is indicated by the grey shaded area.

of-layer (SOL), thus obtaining a relation between the upstream ($T_{e,\text{upstream}} \equiv T_{e,sep}$) and divertor target temperatures ($T_{e,\text{target}}$) [46]. Assuming a conduction limited divertor regime, the upstream temperature at the separatrix can be approximated by the two point model equation [45]:

$$T_{e,\text{upstream}} = \left(T_{e,\text{target}}^{7/2} + \frac{7 P_{sep} L}{2 A_q \kappa} \right)^{\frac{2}{7}}, \tag{4}$$

where L is the connection length, A_q is the projection of the wetted area perpendicular to the heat flux and κ is the parallel heat conductivity coefficient. $T_{e,\text{target}}$ is often neglected as $T_{e,\text{upstream}}^{7/2} \gg T_{e,\text{target}}^{7/2}$ is satisfied in a conduction limited divertor regime. It is common practice to assume that in eq. (4) P_{sep} is the only significantly varying parameter and thus $T_{e,\text{upstream}}$ weakly varies with power ($T_{e,\text{upstream}} \sim P_{sep}^{2/7}$), and approximately equals 100 eV for JET H-modes. However, A_q could also change from discharge to discharge and the condition of the conduction limited divertor regime is not necessarily satisfied in all cases. In the sheath limited regime, the value of $T_{e,\text{target}}^{7/2}$ cannot be neglected. Thus, in realistic experimental conditions, $T_{\text{e,sep}}$ could vary from $\approx$ 100 eV and in extreme cases it might have a non-negligible effect on pedestal stability [47, 48], as it will be discussed in section 5.

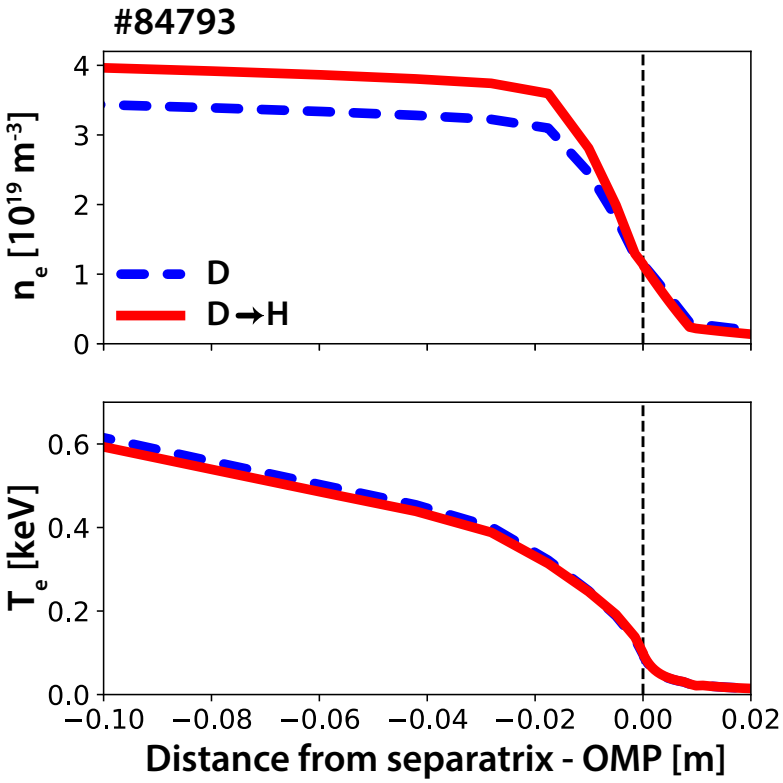

Figure 14. Upstream n_e and T_e profiles from a comparison of EDGE2D-EIRENE simulations where all parameters were kept fixed (transport coefficients, pump albedo, input power, gas fuelling, etc.), but the isotope was changed from D to H.

As highlighted in figure 11, the EDGE2D-EIRENE simulations yield a higher $T_{\mathrm{e,sep}}$ in the selected H discharge ($\approx$ 205 eV) than in the D pulse ($\approx$ 95 eV). This difference is due to the fact that roughly two times more power crosses the separatrix at lower density in the H case. As a result, the H discharge is found to be in the sheath limited regime with $T_{\mathrm{e,upstream}} \approx 205$ eV and $T_{\mathrm{e,target}} \approx 200$ eV in the EDGE2D-EIRENE simulation. In contrast, for the D case $T_{\mathrm{e,upstream}} \approx 95$ eV and $T_{\mathrm{e,target}} \approx 75$ eV. These are still high temperatures at the divertor target, but the temperature drop between upstream and target is larger in the D case than in H. This suggests that the D discharge is closer to the conduction limited regime, while the H discharge is in the sheath limited regime.

The interpretative EDGE2D-EIRENE simulations indicate that $T_{\mathrm{e,sep}}$ is mostly affected by the input power and $\chi_{e,i}$ values in the SOL, which are constrained by the outer target heat flux profile from IR. When both the upstream kinetic profile and outer target heat flux constraints are given, $T_{\mathrm{e,sep}}$ is a robust parameter in the simulation and is not sensitive to the $D_\perp$ and $\chi_{e,i}$ profiles prescribed inside the separatrix. The higher power and lower density in the H discharge compared to the D discharge result in a sheath limited divertor regime in the H case, which leads to high electron temperatures both upstream and at the target. The simulation result suggests higher $T_{\mathrm{e,sep}}$ in H than in D, while $T_{\mathrm{e,sep}}(D) \approx 100$ eV as originally assumed using the 2-point model. We stress that this difference in divertor regime between the two discharges is related to

the density and input power difference in the H and D pair and not to the isotope mass alone. The effect of a possible higher separatrix temperature in H on pedestal stability is discussed in the next section.

The limitations of the EDGE2D-EIRENE simulations are as follows: Cross-field drifts were not taken into account. An edge particle pinch, which may have an important role in the particle transport [34, 35, 36] is not introduced in these simulations. The experimental n_e profile shape could be reproduced with different variations of the diffusion coefficient and the pinch velocity, due to the lack of additional constraints. Although the particle pinch is not taken into account here, its role in edge particle transport is not excluded and is the subject of ongoing research.

In view of the obtained high target temperatures ($T_{\mathrm{e,target}} \approx 200$ eV in the H case) it is important to note that above 100 eV, secondary electron emission could also be important. Secondary electrons are emitted due to high energy plasma particles striking the solid surface. This effect, which would act as an extra electron heat sink in the SOL, is not included in the EDGE2D model. The outer divertor target T_e profile obtained in the EDGE2D-EIRENE simulation for the D case is supported by Langmuir probe measurements, as shown in figure 15. In the H pulse (#91554), due to lack of Langmuir probe measurements, the high $T_{\mathrm{e,target}}$ suggested by the EDGE2D-EIRENE simulation cannot be compared with experiment. The match of the experimental outer target heat flux is less successful in the H case. The somewhat higher heatlfux obtained in EDGE2D-EIRENE than in the experiment may indicate that the obtained target and separatrix temperatures in the H case are an overestimated. Thus, the high $T_{\mathrm{e,sep}} = 205$ eV in EDGE2D-EIRENE for the H discharge should only be taken as an upper limit and must not be considered at face value. Note that these high $T_{\mathrm{e,target}}$ values are not typical of JET-ILW operation but of the low gas fuelling of this particular discharge. It is expected that at higher gas rate (and density) the divertor regime shifts towards conduction limited regime also in H, where lower target and upstream temperatures are expected than those obtained in the EDGE2D-EIRENE simulations for the H discharge at low gas rate analysed here (#91554).

Another limitation is the time independent nature of the EDGE2D-EIRENE simulations, thus the obtained $D_\perp$ represents the total particle transport including the ELM and the inter-ELM particle losses. EDGE2D-EIRENE determine the level of diffusive perpendicular particle transport that provides balance between the sources (NBI fuelling, ionisation and recombination) and sinks. In an ELMy plasma, the sink term consists of inter-ELM transport and ELM losses. These two mechanisms are not treated separately, thus time independent EDGE2D-EIRENE simulations can only give information on the time-averaged effect of inter-ELM and ELM particle transport. It is subject to further studies utilising time dependent simulations to characterise the relative importance of ELM and inter-ELM transport.

The main conclusion of this modelling exercise is that the experimentally observed lower pressure and density pedestal in H compared to D cannot be explained by the changes in neutral penetration, when the isotope mass is changed. In order to match

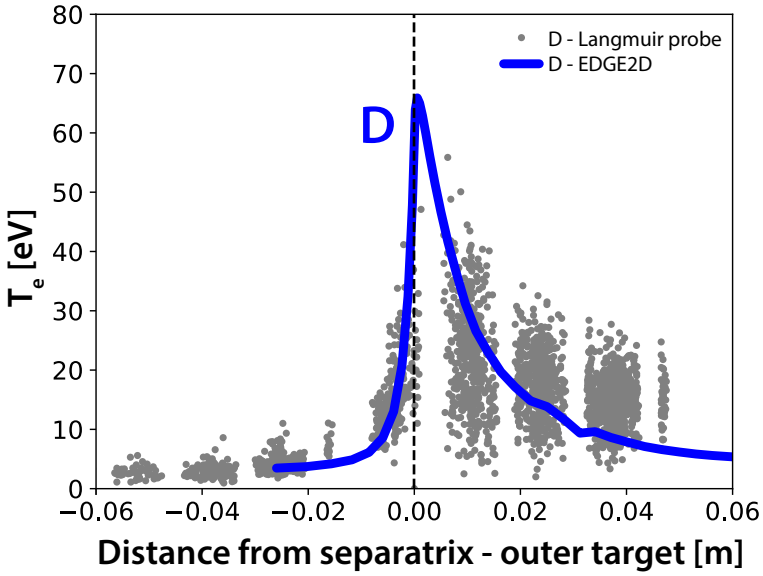

Figure 15. Inter-ELM (40-80 %) outer target T_e profile as evaluated from Langmuir probe measurements for the steady phase of the D pulse #84793 (5.0-6.3 s) in grey and T_e from EDGE2D-EIRENE in blue.

the experimental pedestal profiles, higher perpendicular transport coefficients need to be set for the H pulse compared to D in EDGE2D-EIRENE, indicating that pedestal transport must play a role in setting the different pedestals when the isotope mass is changed. This is consistent with the conclusions of the experimental analysis showing that higher inter-ELM P_{sep} is needed in H compared to D to maintain similar pedestal pressure (see section 3).

5. Linear MHD pedestal stability

Following the analysis of pedestal transport, in this section we discuss whether there is an isotope dependence on linear MHD pedestal stability. A well-known theory which appears to explain the stability conditions of type I ELMy pedestals is the peeling-ballooning (P-B) model [49, 50]. In this model, edge pressure gradient and edge current drive coupled P-B modes, which limit the maximum achievable pedestal gradient and trigger an ELM. In this section the pedestal P-B stability of selected H and D type I ELMy H-modes is examined and the isotope dependence of pedestal stability is discussed.

The linear growth rate (γ_{MHD}) of ideal MHD modes scales as $\sim A^{-1/2}$. In numerical stability codes the stability criterion is often set as a small proportion of the Alfven-frequency $\gamma_{\text{MHD}} > c \times \omega_A$, instead of $\gamma_{\text{MHD}} > 0$. c is typically $\approx 0.02 - 0.05$ and $\omega_A = B_0/(R_0\sqrt{4\pi\rho_0})$ with ρ_0 the mass density. As ω_A and γ_{MHD} scale with isotope mass in the same way, this stability criterion is independent of A.

An isotope dependence of the linear stability is introduced when diamagnetic stabilisation [51] is considered. The diamagnetic drift is expected to stabilise modes - particularly at high toroidal mode number n - when the diamagnetic frequency ($\omega_{\rm dia}$) is comparable to $\gamma_{\rm MHD}$. $\omega_{\rm dia} = m/r \times T_i/(e_i B_0) \times {\rm d}\ln p_i/{\rm d}r$, where T_i, e_i and p_i are temperature, charge, and pressure of the ions, B_0 is the equilibrium magnetic field, r is the minor radius, and m is the poloidal mode number which is linked to the toroidal mode number (n) via the safety factor (q): $m = nq$. Diamagnetic stabilisation can be taken into account in ideal MHD stability analysis by modifying the stability criterion to $\gamma_{\rm MHD} > c \times \omega_{\rm dia}^{\rm max}$ [50, 52]. As $\omega_{\rm dia}^{\rm max}$ is independent of A, but $\gamma_{\rm MHD} \sim A^{-1/2}$, larger isotope mass leads to more stable pedestals when this stability criterion is applied.

Figure 16 shows the $j-\alpha$ pedestal stability diagram for the 3 discharges of section 3 as calculated with HELENA/ELITE [53, 49, 50]. j is the normalised current density self-consistently calculated with HELENA using Sauter's formula [54, 55] for the bootstrap current ($j_{\rm BS}$) and assuming neoclassical resistivity and a fully diffused Ohmic current. Note that Sauter's formula has no isotope mass dependence. α is the normalised pressure gradient as defined in [56]. The inputs for HELENA/ELITE were the fitted kinetic profiles evaluated from Thomson scattering (TS), assuming $T_e = T_i$ (consistent with charge exchange measurements), line averaged Z_{eff} with Be as single impurity. The kinetic profiles here are radially aligned so that the separatrix temperature is 100 eV. The effect of $T_{\rm e,sep}$ on pedestal stability is discussed later in this section.

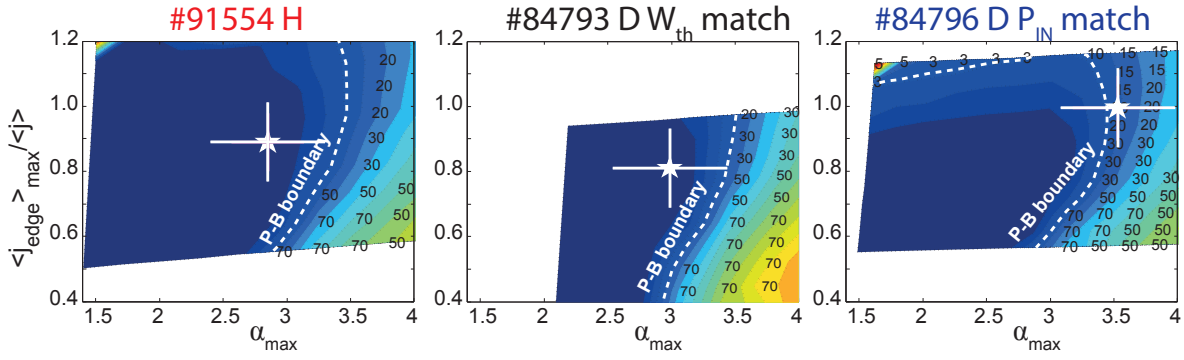

Figure 16. Liner MHD pedestal stability analysis for the hydrogen discharge (#91554) and the two deuterium plasmas matching the total stored energy (#84793) and the input power (#84796) of the hydrogen counterpart. $I_p = 1.4$ MA, $B_t = 1.7$ T. The numbers indicate the most unstable mode number at given edge current and pressure gradient.

In figure 16, the stability boundary (white dashed lines) is obtained using $\gamma_{\rm MHD} > 0.03 \times \omega_A$ stability criterion. The white stars show the operational point of the pedestal as obtained in the experiment. The pedestals in these low gas rate ($\Gamma = 3 \cdot 10^{21}$ e/s) H and D type I ELMy H-modes are close to the P-B boundary within the uncertainties of the operational point. The pedestal collisionality is higher in the high power D pulse (#84796) than in the other two plasmas and thus the operational point is somewhat closer to the peeling boundary. Although the mode number of the most unstable mode

($n = 20$) is consistent with the pedestal being ballooning limited. This observation is confirmed with the same analysis performed on a wider dataset, although H pedestals tend to be on the stable side of the stability boundary. At medium and high gas rate, the operational point moves to the stable region in H, which is similar to what has been found in D at high input power [20]. Pedestals of the 1.0 MA/1.0 T dataset at medium gas are also stable to P-B modes both in H and D, especially at higher power.

The effect of diamagnetic stabilisation is investigated by performing linear ideal MHD stability analysis with HELENA/ELITE on the hydrogen pedestal. Figure 17 shows the j-α stability diagram for H shot #91554 profiles using $\gamma_{\mathrm{MHD}} > 0.25 \times \omega_{\mathrm{dia}}^{\mathrm{max}}$ as stability criterion, assuming $A = 2$ (dashed blue line) and $A = 1$ (solid red line) isotope. When diamagnetic stabilisation is taken into account, the stable region shrinks from $A = 2$ to $A = 1$ in the calculations indicating less stable pedestals for H than for D with the same input profiles. The critical pedestal pressure height can be evaluated by scaling up and down the experimental pressure profile and calculating the associated current profile self-consistently. The pressure profile which is closest to marginal stability gives the critical pressure gradient. The difference between the stability boundaries when the isotope mass is changed from $A = 2$ to $A = 1$ for discharge #91554 translates to ≈ 4 % reduction in the critical pedestal pressure height. Thus, the isotope dependence of linear MHD stability is small and alone does not explain the higher pedestal pressure observed in D type I ELMy H-modes compared to H in JET-ILW.

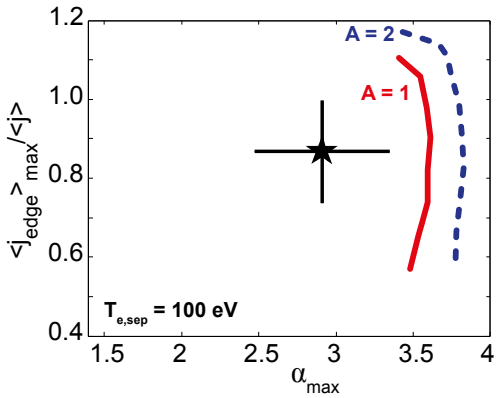

Figure 17. P-B stability of the pre-ELM pedestal of H type-I ELMy H-mode #91554 as calculated with HELENA/ELITE with the stability criterion $\gamma_{\mathrm{MHD}} > 0.25 \times \omega_{\mathrm{dia}}^{\mathrm{max}}$. The black star indicates the operational point. The blue dashed line shows the stability boundary assuming $A = 2$. The stable region shrinks when the isotope mass is changed from D (blue dashed line) to H (red solid line). The kinetic profiles are radially aligned so that $T_{e,sep} = 100$ eV.

The effect of diamagnetic stabilisation on JET pedestals has already been demonstrated using a more rigorous treatment of the diamagnetic drift with an extended MHD model [57, 58]. This approach could be the subject of further studies, however, the results of ideal MHD based estimate used in the present work suggests that only a weak isotope dependence is expected. The effect of sheared rotation on pedestal stability [59]

is not discussed here, but it may lead to differences in the pedestal stability between H and D plasmas as for example the different input power to achieve the same pedestal pressure in H and D (see section 2) could lead to differences in the NBI torque and thus in the sheared rotation.

While so far we have investigated the pedestal stability utilising the common assumption of $T_{\mathrm{e,sep}} = 100$ eV (widely used in the literature [37, 38, 39, 40, 41, 42, 43]) for both H and D cases, we now assess from a qualitative point of view the effect of a potentially higher $T_{e,sep}$ in H on pedestal stability as suggested by the interpretative EDGE2D-EIRENE simulations presented in section 4. The simulations indicated that due to the high power and low density in the H pulse, the divertor may be in sheath limited regime when the $T_{\mathrm{e,sep}} \sim P^{2/7}$ scaling breaks down and $T_{\mathrm{e,sep}}$ could be much higher than 100 eV. A sensitivity test is carried out here to assesses the effect of $T_{\mathrm{e,sep}} > 100$ eV on pedestal stability. The linear ideal MHD stability analysis for the hydrogen pulse #91554 is shown in figure 18a, assuming $T_{\mathrm{e,sep}} = 100$ eV (solid black), $T_{\mathrm{e,sep}} = 150$ eV (dotted green) and $T_{\mathrm{e,sep}} = 200$ eV (dashed magenta) as a sensitivity test. The difference in boundary condition at the separatrix translates into significant differences in the P-B stability boundary, with both ballooning and peeling boundaries shrinking due to destabilisation of P-B modes as $T_{\mathrm{e,sep}}$ is increased, similarly to the analysis reported in [48]. As illustrated in figure 18b, the higher $T_{e,sep}$ shifts the maximum pressure gradient closer to the separatrix, thus moving to a region of higher magnetic shear, which leads to destabilisation of ballooning modes. At the same time, the edge current profile - which is dominated by the bootstrap current - is also shifted radially outward, leading to higher current at the separatrix, which destabilises peeling modes. The difference in the critical pedestal pressure height between $T_{e,sep} \approx 100$ eV and 200 eV cases is approximately 15 %. This change is qualitatively consistent with type I ELMs being triggered at lower pedestal pressures in the H case (typically originating from lower density). As described in section 4, however, such high $T_{\mathrm{e,sep}}$ in the H discharge is unrealistic, but the qualitative picture illustrated here warrants further investigation and the need for direct measurement of $T_{\mathrm{e,sep}}$ when the isotope mass is changed.

6. Summary and future work

In the present paper, the pedestal structure, linear MHD stability and ELM losses have been analysed to gain insight on the dependence of JET-ILW type I ELMy pedestals on isotope mass. The pedestal pressure is typically reduced in H compared to D at the same input power and gas rate, primarily due to lower pedestal density in H.

It has been concluded that higher ELM and/or inter-ELM transport and pedestal stability is likely to be the main player in setting the difference between H and D pedestals and not the neutral penetration. EDGE2D-EIRENE simulations indicated that the pedestal density changes opposite to the experimental observations when the effect of neutral penetration is investigated. Interpretative EDGE2D-EIRENE analysis

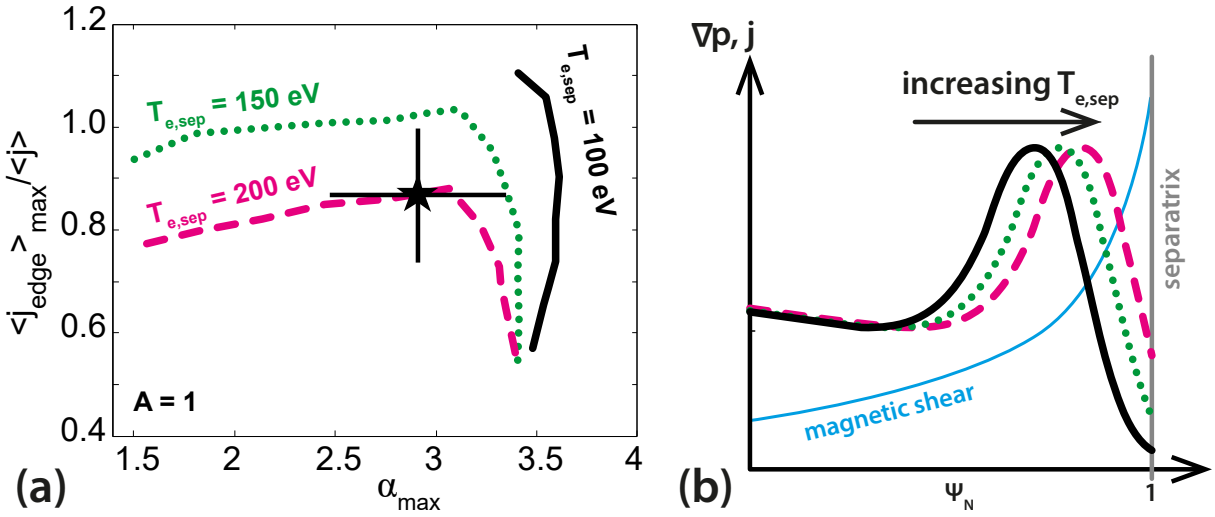

Figure 18. (a) Effect of $T_{\mathrm{e,sep}}$ on P-B stability of the pre-ELM pedestal of discharge #91554 as calculated with HELENA/ELITE using the stability criterion $\gamma_{\mathrm{MHD}} > 0.25 \times \omega_{\mathrm{dia}}^{\mathrm{max}}$. The black star indicates the operational point of the pedestal for #91554. The stability boundary is shown assuming $T_{\mathrm{e,sep}} = 100$ eV (solid black), $T_{\mathrm{e,sep}} = 150$ eV (dotted green) and $T_{\mathrm{e,sep}} = 200$ eV (dashed magenta). (b) Illustration of the maximum pressure gradient and edge current moving radially outwards, closer to the separatrix with increasing $T_{\mathrm{e,sep}}$ to a region with higher magnetic shear.

for a selected pair of discharges showed that the edge transport needs to be increased in H compared to D to explain the experiments. This is also supported by the power balance analysis, showing that the inter-ELM separatrix loss power is higher in H than in D at similar pedestal top pressure.

Pedestal linear MHD stability has been investigated with HELENA/ELITE in H and D, showing that P-B modes are more unstable at lower isotope mass. The direct isotope dependence of linear MHD pedestal stability becomes apparent when the diamagnetic frequency is included in the stability criterion to account for its stabilisation effect. P-B modes are more stable in D than in H, but the effect is small and alone does not explain the higher pedestal pressure observed in D. Interpretative EDGE2D-EIRENE simulations indicate that the electron temperature at the separatrix could be higher in H than in D due to different divertor conditions in a pair of type I ELMy H-modes with similar stored energy achieved at twice the power in H, at low gas rate. The largest difference in boundary conditions at the separatrix between H and D translates into significant destabilisation of P-B modes for the H pedestal compared to D. This effect is qualitatively consistent with type I ELMs being triggered at lower pedestal densities in the H case, although the $T_{\mathrm{e,sep}}$ value in the sensitivity test was chosen as an extreme case and should not be considered at face value in the analysed H and D pair. The physics mechanism underlying the profile changes at the plasma edge when the isotope mass is varied is not yet understood. Note that direct measurement of the separatrix temperature would be needed in order to confirm or disprove the higher indicated $T_{\mathrm{e,sep}}$ in H than in D for the selected pulses analysed.

The results presented in this paper indicate that ELM and/or inter-ELM transport and, to a lesser extent, pedestal stability are likely to be affected by the isotope mass, leading to a favourable isotope dependence of pedestal confinement. Further studies are required to be able to provide quantitative predictions beyond the qualitative findings of this work. Future work should include further studies to examine the role of the particle source and transport in setting the density pedestal with different isotopes. These will also investigate the relative importance of ELM and inter-ELM particle losses by utilising time dependent simulations with simplified ELM models. Further experiments are planned in the upcoming JET campaigns to examine the ELM particle losses in different isotopes by applying ELM trigger techniques to match the ELM frequency in H, D and T plasmas. Upcoming T and DT experiments are devoted to elucidate the isotope dependence of the pedestal by decoupling changes in ELM frequency and isotope mass for the same input parameters. Experimental analysis and interpretative edge transport analysis suggest that the pedestal transport is likely to play an important role in setting the pedestal height and shape and may be the primary difference between H and D pedestals. Thus, future work should also focus on studying the turbulence driving the inter-ELM pedestal transport with gyrokinetic simulations.

Acknowledgments

The first author would like to thank M. Groth for fruitful discussions. This work was supported by the Engineering and Physical Sciences Research Council [EP/L01663X/1]. This work has been carried out within the framework of the EUROfusion Consortium and has received funding from the Euratom research and training programme 2014-2018 and 2019-2020 under grant agreement No 633053. The views and opinions expressed herein do not necessarily reflect those of the European Commission.

Appendix A. Pump albedo in EDGE2D-EIRENE for H and D

In the simulations, the pumping surfaces were placed at the corners of the simulated divertor (see figure C1b in Appendix C), where - in experiment - neutrals would be moving into the sub-divertor region by the action of the cryopump. The pump efficiency is defined by the pump albedo, which gives the probability that a neutral - which reaches the pumping surface - is reflected. The pump albedo was set to 0.4 for H and to 0.7 for D to obtain a match of the upstream profiles for these two discharges. However, these values are not consistent with testbed results on the sticking coefficients (α_s) of H_2 and D_2 at a cryopump surface [60, 61]. The sticking coefficient is the ratio of the number of particles sticking to the cryosurface related to the total number of particles impinging on it. The sub-divertor structures and the cryopump are not modelled in these EIRENE simulations, thus a one-to-one comparison between the albedo defined in EDGE2D-EIRENE and the testbed results for the sticking coefficients on a cryosurface is not possible, but the albedo is roughly proportional to $(1 - \alpha_s)$. The testbed results

show that the sticking coefficient is higher in D than in H [60, 61], implying lower albedo in D than in H in contrast to the EDGE2D-EIRENE pump albedo settings. A possible reason for this disagreement could be that the much hotter ions, electrons and neutrals in the SOL of the H discharge may have resulted in different neutral recycling at the wall.

Appendix B. V/H vs C/C divertor configuration

The impact of divertor configuration (C/C vs V/H) on the pedestal density has been investigated in a separate study, where all input parameters of the interpretative simulation for #84793 (transport coefficients, pump albedo, input power, gas fuelling, etc.) were kept fixed, but the divertor configuration was changed from C/C to V/H. The pedestal density increased by approximately 20 %, while $T_{\mathrm{e,PED}}$ decreased leading to virtually no change in pedestal pressure as shown in figure B1a. This is consistent with the experimental observations in figure B1b, where $n_{\mathrm{e,PED}}$ is shown as a function of P_{sep} for a subset of the JET-ILW H and D isotope dataset at low gas rate, relevant for the comparison of different divertor configurations. $n_{\mathrm{e,PED}}$ is approximately 20 % larger in V/H than in C/C as represented by the dashed black lines in figure B1b. Note that the difference in $n_{\mathrm{e,PED}}$ between the H and D pulses (#91554 and #84793, see figure 4) investigated in section 4 is much higher - approximately 50 % - than what could be attributed to the different divertor configurations.

Appendix C. Grid and vessel wall definition in EDGE2D-EIRENE for C/C divertor configuration

For the C/C divertor configuration grid in EDGE2D-EIRENE, the wall structure had to be slightly modified around the outer strike-point so that the grid does not cross wall surfaces, as shown in figure C1b. In this way, the real JET divertor geometry (in green) is slightly altered to be aligned with the outermost grid elements. This modification could possibly lead to some differences in the neutral pressure around the outer strike point compared to that in the real geometry, but the aim here was to compare a pair of H and D simulations and not to carry out comprehensive validation of the code. Thus, both the H and the D cases were simulated using the same grid. A quantitative answer on how much the wall structure alteration used here affects the simulated target and upstream profiles could only be given by testing this effect with an edge transport code such as SolEdge2D [62, 63] that is capable of handling complex geometries, but this is out of the scope of the present work.

References

[1] C.F. Maggi, H. Weisen, J.C. Hillesheim, A. Chankin, E. Delabie, L. Horvath, F. Auriemma, I.S. Carvalho, G. Corrigan, J. Flanagan, L. Garzotti, D. Keeling, D. King, E. Lerche, R. Lorenzini, M. Maslov, S. Menmuir, S. Saarelma, A.C.C. Sips, E.R. Solano, E. Belonohy, F.J. Casson,

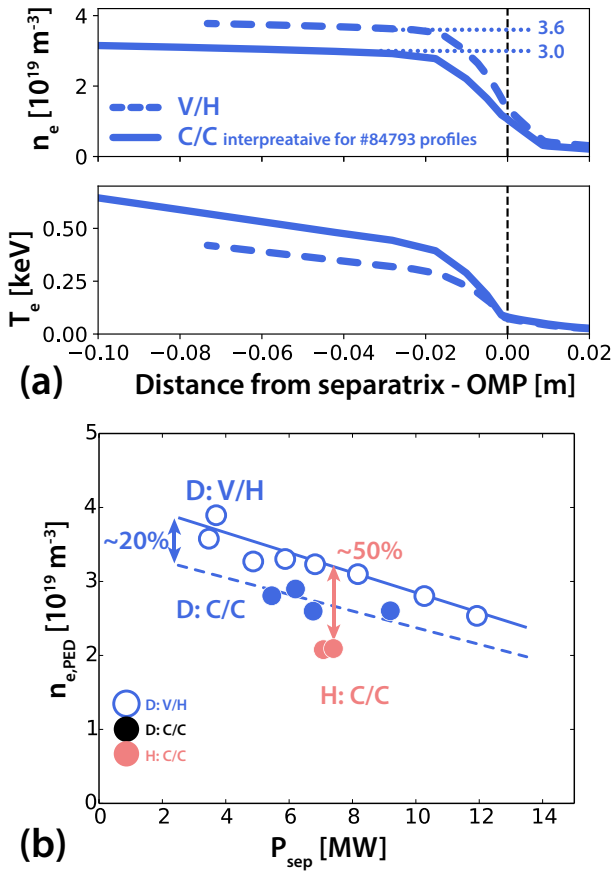

Figure B1. (a) Upstream n_e and T_e profiles of a pair EDGE2D-EIRENE simulations where all parameters were kept fixed (transport coefficients, pump albedo, input power, gas fuelling, etc.), but the divertor configuration was changed from C/C to V/H. (b) $n_{\mathrm{e,PED}}$ as a function of P_{sep} for a subset of the JET-ILW H and D isotope dataset at low gas rate, relevant for the comparison of different divertor configurations.

C. Challis, C. Giroud, V. Parail, C. Silva, M. Valisa, and JET Contributors. Isotope effects on L-H threshold and confinement in tokamak plasmas. *Plasma Physics and Controlled Fusion*, 60(1):014045, 2018.

[2] F. Wagner, G. Becker, K. Behringer, D. Campbell, A. Eberhagen, W. Engelhardt, G. Fussmann, O. Gehre, J. Gernhardt, G.V. Gierke, G. Haas, M. Huang, F. Karger, M. Keilhacker, O. Klüber, M. Kornherr, K. Lackner, G. Lisitano, G.G. Lister, H.M. Mayer, D. Meisel, E.R. Müller, H. Murmann, H. Niedermeyer, W. Poschenrieder, H. Rapp, H. Röhr, F. Schneider, G. Siller, E. Speth, A. Stäbler, K.H. Steuer, G. Venus, O. Vollmer, and Z. Yü. Regime of improved confinement and high beta in neutral-beam-heated divertor discharges of the ASDEX tokamak. *Phys. Rev. Lett.*, 49:1408–1412, 1982.

[3] H. Urano, T. Takizuka, Y. Kamada, N. Oyama, H. Takenaga, and the JT-60 Team. Dimensionless parameter dependence of H-mode pedestal width using hydrogen and deuterium plasmas in JT-60U. *Nuclear Fusion*, 48(4):045008, 2008.

[4] H. Urano, T. Takizuka, T. Fujita, Y. Kamada, T. Nakano, N. Oyama, and the JT-60 Team. Energy confinement of hydrogen and deuterium H-mode plasmas in JT-60U. *Nuclear Fusion*, 52(11):114021, 2012.

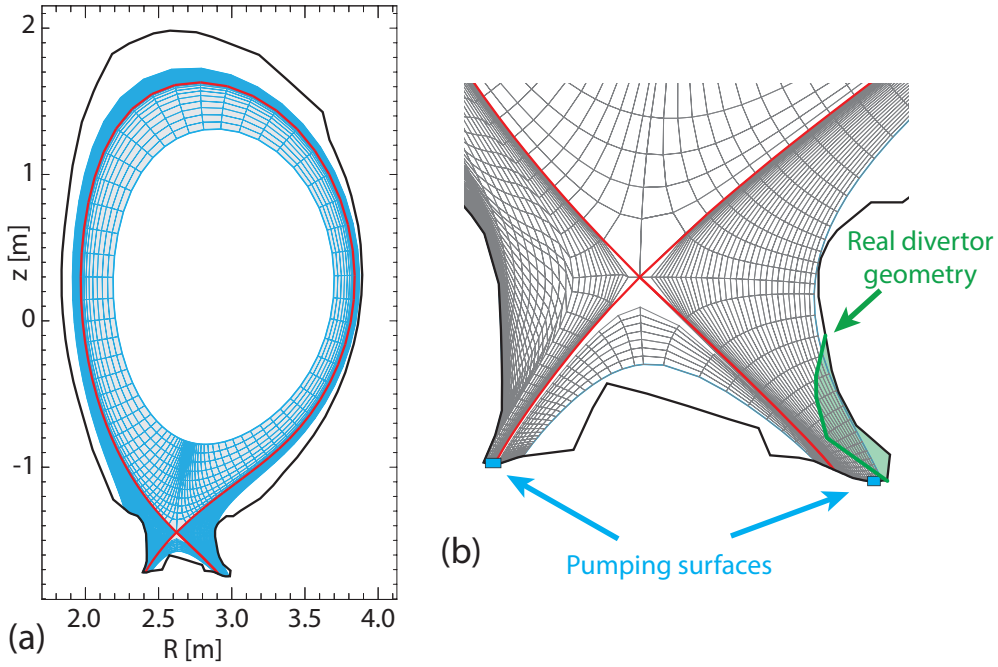

Figure C1. (a) The EDGE2D simulation grid in cyan. (b) The real divertor geometry (in green) is slightly altered at the outer strike point to be aligned with the outermost grid elements. The pump surfaces are shown in cyan close to the strike points.

[5] H. Urano, T. Takizuka, N. Aiba, M. Kikuchi, T. Nakano, T. Fujita, N. Oyama, Y. Kamada, N. Hayashi, and the JT-60 Team. Hydrogen isotope effects on ITG scale length, pedestal and confinement in JT-60 H-mode plasmas. *Nuclear Fusion*, 53(8):083003, 2013.

[6] D.P. Schissel, K.H. Burrell, J.C. DeBoo, R.J. Groebner, A.G. Kellman, N. Ohyabu, T.H. Osborne, M. Shimada, R.T. Snider, R.D. Stambaugh, T.S. Taylor, and DIII-D Research Team. Energy confinement properties of H-mode discharges in the DIII-D tokamak. *Nuclear Fusion*, 29(2):185–197, feb 1989.

[7] ASDEX Team. The H-Mode of ASDEX. *Nuclear Fusion*, 29(11):1959–2040, 1989.

[8] M. Bessenrodt-Weberpals, F. Wagner, O. Gehre, L. Giannone, J.V. Hofmann, A. Kallenbach, K. McCormick, V. Mertens, H.D. Murmann, F. Ryter, B.D. Scott, G. Siller, F.X. Soldner, A. Stabler, K.H. Steuer, U. Stroth, N. Tsois, H. Verbeek, and H. Zohm. The isotope effect in ASDEX. *Nuclear Fusion*, 33(8):1205–1238, 1993.

[9] F.M. Laggner, E. Wolfrum, M. Cavedon, F. Mink, M. Bernert, M.G. Dunne, P.A. Schneider, A. Kappatou, G. Birkenmeier, R. Fischer, M. Willensdorfer, F. Aumayr, EUROfusion MST1 Team, and ASDEX Upgrade Team. Pedestal structure and inter-ELM evolution for different main ion species in ASDEX Upgrade. *Physics of Plasmas*, 24(5):056105, 2017.

[10] C.F. Maggi, H. Weisen, F.J. Casson, F. Auriemma, R. Lorenzini, H. Nordman, E. Delabie, F. Eriksson, J. Flanagan, D. Keeling, D. King, L. Horvath, S. Menmuir, A. Salmi, G. Sips, T. Tala, and I. Voitsekhovich and. Isotope identity experiments in JET-ILW with h and d l-mode plasmas. *Nuclear Fusion*, 59(7):076028, jun 2019.

[11] A V Chankin, G Corrigan, and C F Maggi and. EDGE2d-EIRENE simulations of the influence of isotope effects and anomalous transport coefficients on near scrape-off layer radial electric field. *Plasma Physics and Controlled Fusion*, 61(7):075010, may 2019.

[12] P. A. Schneider, A. Bustos, P. Hennequin, F. Ryter, M. Bernert, M. Cavedon, M. G. Dunne, R. Fischer, T. GÃűrler, T. Happel, V. Igochine, B. Kurzan, A. Lebschy, R.M. McDermott, P. Morel, M. Willensdorfer, and and. Explaining the isotope effect on heat transport in L-mode

with the collisional electron-ion energy exchange. *Nuclear Fusion*, 57(6):066003, 2017.

[13] S. M. Kaye, M. Greenwald, U. Stroth, O. Kardaun, A. Kus, D Schissel, J DeBoo, G Bracco, K Thomsen, J.G Cordey, Y Miura, T Matsuda, H Tamai, T Takizuda, T Hirayama, H Kikuchi, O Naito, A Chudnovskij, J Ongena, and G Hoang. ITER L mode confinement database. *Nuclear Fusion*, 37(9):1303–1328, 1997.

[14] H. Yamada, K. Tanaka, R. Seki, C. Suzuki, K. Ida, K. Fujii, M. Goto, S. Murakami, M. Osakabe, T. Tokuzawa, M. Yokoyama, M. Yoshinuma, and LHD Experiment Group. Isotope effect on energy confinement time and thermal transport in neutral-beam-heated stellarator-heliotron plasmas. *Phys. Rev. Lett.*, 123:185001, Oct 2019.

[15] K. Nagaoka, H. Takahashi, M. Nakata, S. Satake, K. Tanaka, K. Mukai, M. Yokoyama, H. Nakano, S. Murakami, K. Ida, M. Yoshinuma, S. Ohdachi, T. Bando, M. Nunami, R. Seki, H. Yamaguchi, M. Osakabe, and T. Morisaki and. Transport characteristics of deuterium and hydrogen plasmas with ion internal transport barrier in the large helical device. *Nuclear Fusion*, 59(10):106002, aug 2019.

[16] J.G. Cordey, B. Balet, D.V. Bartlett, R.V. Budny, J.P. Christiansen, G.D. Conway, L.-G. Eriksson, G.M. Fishpool, C.W. Gowers, J.C.M. de Haas, P.J. Harbour, L.D. Horton, A.C. Howman, J. Jacquinot, W. Kerner, C.G. Lowry, R.D. Monk, P. Nielsen, E. Righi, F.G. Rimini, G. Saibene, R. Sartori, B. Schunke, A.C.C. Sips, R.J. Smith, M.F. Stamp, D.F.H. Start, K. Thomsen, B.J.D. Tubbing, and M.G. von Hellermann. Plasma confinement in JET H mode plasmas with H, D, DT and T isotopes. *Nuclear Fusion*, 39(3):301, 1999.

[17] M. Maslov, A. Boboc, M. Brix, J.C. Flanagan, E. Peluso, C. Price, and M. Romanelli and. Energy and particle confinement in JET H-mode plasma. *Nuclear Fusion*, 60(3):036007, jan 2020.

[18] H. Weisen, C.F. Maggi, L. Horvath, F. Auriemma, T.W. Bache, F.J. Casson, A. Chankin, E. Delabie, C. Giroud, D. King, R. Lorenzini, S. Menmuir, and E. Viezzer. Isotope dependence of confinement in JET Deuterium and Hydrogen plasmas. In *27th IAEA Fusion Energy Conference, Ahmedabad, India*, pages EX/P1–4, 2018.

[19] H. Weisen, C. F. Maggi, M. Oberparleiter, F. J. Casson, Y. Camenen, S. Menmuir, L. Horvath, F. Auriemma, T. W. Bache, N. Bonanomi, and et al. Isotope dependence of energy, momentum and particle confinement in tokamaks. *Journal of Plasma Physics*, 86(5):905860501, 2020.

[20] C.F. Maggi, S. Saarelma, F.J. Casson, C. Challis, E. de la Luna, L. Frassinetti, C. Giroud, E. Joffrin, J. Simpson, M. Beurskens, I. Chapman, J. Hobirk, M. Leyland, P. Lomas, C. Lowry, I. Nunes, F. Rimini, A.C.C. Sips, H. Urano, and JET Contributors. Pedestal confinement and stability in JET-ILW ELMy H-modes. *Nuclear Fusion*, 55(11):113031, 2015.

[21] C.F. Maggi, L. Frassinetti, L. Horvath, A. Lunniss, S. Saarelma, H. Wilson, J. Flanagan, M. Leyland, I. Lupelli, S. Pamela, H. Urano, L. Garzotti, E. Lerche, I. Nunes, F. Rimini, and JET Contributors. Studies of the pedestal structure and inter-ELM pedestal evolution in JET with the ITER-like wall. *Nuclear Fusion*, 57(11):116012, 2017.

[22] V.P. Bhatnagar, J. Lingertat, R. Barnsley, P. Breger, J.P. Christiansen, S. Clement, J.G. Cordey, S.J. Davies, J.K. Ehrenberg, L.G. Eriksson, G.M. Fishpool, P.J. Harbour, L.D. Horton, J. Jacquinot, H.J. JÃd'ckel, K. Lawson, C.G. Lowry, C.F. Maggi, G.F. Matthews, R.D. Monk, D.P. OBrien, V.V. Parail, E. Righi, G. Saibene, R. Sartori, B. Schunke, A.C.C. Sips, M.F. Stamp, D.F.H. Start, and K. Thomsen. Edge localized modes and edge pedestal in NBI and ICRF heated H, D and T plasmas in JET. *Nuclear Fusion*, 39(3):353–367, 1999.

[23] R.J. Groebner and T.H. Osborne. Scaling studies of the high mode pedestal. *Physics of Plasmas*, 5(5):1800–1806, 1998.

[24] R. Pasqualotto, P. Nielsen, C. Gowers, M. Beurskens, M. Kempenaars, T. Carlstrom, D. Johnson, and JET-EFDA Contributors. High resolution Thomson scattering for Joint European Torus (JET). *Review of Scientific Instruments*, 75(10):3891–3893, 2004.

[25] L. Frassinetti, M.N.A. Beurskens, R. Scannell, T.H. Osborne, J. Flanagan, M. Kempenaars, M. Maslov, R. Pasqualotto, M. Walsh, and JET-EFDA Contributors. Spatial resolution of the JET Thomson scattering system. *Review of Scientific Instruments*, 83(1), 2012.

[26] M.J. Leyland, M.N.A. Beurskens, J.C. Flanagan, L. Frassinetti, K.J. Gibson, M. Kempenaars, M. Maslov, R. Scannell, and JET Contributors. Edge profile analysis of Joint European Torus (JET) Thomson scattering data: Quantifying the systematic error due to edge localised mode synchronisation. *Review of Scientific Instruments*, 87(1), 2016.

[27] L. Frassinetti, D. Dodt, M.N.A. Beurskens, A. Sirinelli, J.E. Boom, T. Eich, J. Flanagan, C. Giroud, M.S. Jachmich, M. Kempenaars, P. Lomas, G. Maddison, C. Maggi, R. Neu, I. Nunes, C. Perez von Thun, B. Sieglin, M. Stamp, and JET-EFDA Contributors. Effect of nitrogen seeding on the energy losses and on the time scales of the electron temperature and density collapse of type-I ELMs in JET with the ITER-like wall. *Nuclear Fusion*, 55(2):023007, 2015.

[28] A. Loarte, M. Becoulet, G. Saibene, R. Sartori, D.J. Campbell, T. Eich, A. Herrmann, M. Laux, W. Suttrop, B. Alper, P.J. Lomas, G. Matthews, S. Jachmich, J. Ongena, P. Innocente, and EFDA-JET Workprogramme Collaborators. Characteristics and scaling of energy and particle losses during Type I ELMs in JET H-modes. *Plasma Physics and Controlled Fusion*, 44(9):1815–1844, 2002.

[29] A. Loarte, G. Saibene, R. Sartori, D. Campbell, M. Becoulet, L. Horton, T. Eich, A. Herrmann., G. Matthews, N. Asakura, A. Chankin, A. Leonard, G. Porter, G. Federici, G. Janeschitz, M. Shimada, and M. Sugihara. Characteristics of type I ELM energy and particle losses in existing devices and their extrapolation to ITER. *Plasma Physics and Controlled Fusion*, 45(9):1549–1569, 2003.

[30] A. Boboc, M. Gelfusa, A. Murari, P. Gaudio, and JET-EFDA Contributors. Recent developments of the JET far-infrared interferometer-polarimeter diagnostic. *Review of Scientific Instruments*, 81(10):10D538, 2010.

[31] D. Reiter. Progress in two-dimensional plasma edge modelling. *Journal of Nuclear Materials*, 196-198:80–89, 1992.

[32] R. Simonini, G. Corrigan, G. Radford, J. Spence, and A. Taroni. Models and numerics in the multi-fluid 2-D edge plasma code EDGE2D/U. *Contributions to Plasma Physics*, 34(2-3):368–373, 1994.

[33] S. Wiesen. EDGE2D/EIRENE code interface report. *IRC Report*, 2006. http://www.eirene.de/e2deir_report_30jun06.pdf.

[34] H. Weisen, A. Zabolotsky, M. Maslov, M. Beurskens, C. Giroud, D. Mazon, and JET-EFDA contributors. Scaling of density peaking in JET H-modes and implications for ITER. *Plasma Physics and Controlled Fusion*, 48(5A):A457–A466, 2006.

[35] C. Angioni, E. Fable, M. Greenwald, M. Maslov, A.G. Peeters, H. Takenaga, and H. Weisen. Particle transport in tokamak plasmas, theory and experiment. *Plasma Physics and Controlled Fusion*, 51(12):124017, 2009.

[36] A. Loarte, M.J. Leyland, J.A. Mier, M.N.A. Beurskens, I. Nunes, V. Parail, P.J. Lomas, G.R. Saibene, R.I.A. Sartori, and L. Frassinetti and. Plasma density and temperature evolution following the H-mode transition at JET and implications for ITER. *Nuclear Fusion*, 53(8):083031, jul 2013.

[37] M.J. Leyland, M.N.A. Beurskens, L. Frassinetti, T. Osborne, P.B. Snyder, C. Giroud, S. Jachmich, G. Maddison, P. Lomas, C. Perez von Thun, S. Saarelma, G. Saibene, and K.J. Gibson. Pedestal study across a deuterium fuelling scan for high triangularity ELMy h-mode plasmas on JET with the carbon wall. *Nuclear Fusion*, 53(8):083028, jul 2013.

[38] E. Stefanikova, L. Frassinetti, S. Saarelma, A. Loarte, I. Nunes, L. Garzotti, P. Lomas, F. Rimini, P. Drewelow, U. Kruezi, B. Lomanowski, E. de la Luna, L. Meneses, M. Peterka, B. Viola, C. Giroud, C.F. Maggi, and JET contributors. Effect of the relative shift between the electron density and temperature pedestal position on the pedestal stability in JET-ILW and comparison with JET-C. *Nuclear Fusion*, 58(5):056010, 2018.

[39] L. Frassinetti, M.G. Dunne, U. Sheikh, S. Saarelma, C.M. Roach, E. Stefanikova, C. Maggi, L. Horvath, S. Pamela, E. de la Luna, E. Wolfrum, M. Bernert, P. Blanchard, B. Labit, A. Merle, L. Guimarais, S. Coda, H. Meyer, J.C. Hillesheim, the ASDEX Upgrade Team, JET

Contributors, the TCV Team, and the EUROfusion MST1 Team. Role of the pedestal position on the pedestal performance in AUG, JET-ILW and TCV and implications for ITER. *Nuclear Fusion*, 59(7):076038, 2019.

[40] S. Saarelma, L. Frassinetti, P. Bilkova, C. D. Challis, A. Chankin, R. FridstrÃűm, L. Garzotti, L. Horvath, and C. F. Maggi. Self-consistent pedestal prediction for JET-ILW in preparation of the DT campaign. *Physics of Plasmas*, 26(7):072501, 2019.

[41] M G Dunne, S Potzel, F Reimold, M Wischmeier, E Wolfrum, L Frassinetti, M Beurskens, P Bilkova, M Cavedon, R Fischer, B Kurzan, F M Laggner, R M McDermott, G Tardini, E Trier, E Viezzer, and M Willensdorfer. The role of the density profile in the ASDEX-upgrade pedestal structure. *Plasma Physics and Controlled Fusion*, 59(1):014017, oct 2016.

[42] H J Sun, E Wolfrum, B Kurzan, T Eich, K Lackner, A Scarabosio, I Paradela Pérez, O Kardaun, M Faitsch, S Potzel, and U Stroth. Study of near SOL decay lengths in ASDEX Upgrade under attached and detached divertor conditions. *Plasma Physics and Controlled Fusion*, 59(10):105010, aug 2017.

[43] R.J. Groebner, T.H. Osborne, A.W. Leonard, and M.E. Fenstermacher. Temporal evolution of H-mode pedestal in DIII-D. *Nuclear Fusion*, 49(4):045013, mar 2009.

[44] P.C. Stangeby. *The Plasma Boundary of Magnetic Fusion Devices*. Series in Plasma Physics and Fluid Dynamics. Taylor & Francis, 2000.

[45] A. Kallenbach, N. Asakura, A. Kirk, A. Korotkov, M.A. Mahdavi, D. Mossessian, and G.D. Porter. Multi-machine comparisons of h-mode separatrix densities and edge profile behaviour in the ITPA SOL and Divertor Physics Topical Group. *Journal of Nuclear Materials*, 337-339:381–385, 2005.

[46] J Neuhauser, D Coster, H U Fahrbach, J C Fuchs, G Haas, A Herrmann, L Horton, M Jakobi, A Kallenbach, M Laux, J W Kim, B Kurzan, H W MÃijller, H Murmann, R Neu, V Rohde, W Sandmann, W Suttrop, E Wolfrum, and the ASDEX Upgrade Team. Transport into and across the scrape-off layer in the ASDEX Upgrade divertor tokamak. *Plasma Physics and Controlled Fusion*, 44(6):855–869, may 2002.

[47] J. Simpson, D. Moulton, C. Giroud, M. Groth, and G. Corrigan. Using EDGE2D-EIRENE to simulate the effect of impurity seeding and fueling on the upstream electron separatrix temperature. *Nuclear Materials and Energy*, 20:100599, 2019.

[48] S. Saarelma, A. Järvinen, M. Beurskens, C. Challis, L. Frassinetti, C. Giroud, M. Groth, M. Leyland, C.F. Maggi, J. Simpson, and JET Contributors. The effects of impurities and core pressure on pedestal stability in Joint European Torus (JET). *Physics of Plasmas*, 22(5):056115, 2015.

[49] H.R. Wilson, P.B. Snyder, G.T.A. Huysmans, and R.L. Miller. Numerical studies of edge localized instabilities in tokamaks. *Physics of Plasmas*, 9(4):1277–1286, 2002.

[50] P.B. Snyder, H.R. Wilson, J.R. Ferron, L.L. Lao, A.W. Leonard, T.H. Osborne, A.D. Turnbull, D. Mossessian, M. Murakami, and X.Q. Xu. Edge localized modes and the pedestal: A model based on coupled peelingâĂŞballooning modes. *Physics of Plasmas*, 9(5):2037–2043, 2002.

[51] G.T.A. Huysmans, S.E. Sharapov, A.B. Mikhailovskii, and W. Kerner. Modeling of diamagnetic stabilization of ideal magnetohydrodynamic instabilities associated with the transport barrier. *Physics of Plasmas*, 8(10):4292–4305, 2001.

[52] P.B. Snyder, R.J. Groebner, J.W. Hughes, T.H. Osborne, M. Beurskens, A.W. Leonard, H.R. Wilson, and X.Q. Xu. A first-principles predictive model of the pedestal height and width: development, testing and ITER optimization with the EPED model. *Nuclear Fusion*, 51(10):103016, 2011.

[53] G.T.A. Huysmans, J.P. Goedbloed, and W. Kerner. Isoparametric bicubic Hermite elements for solution of the Grad-Shafranov equation. In *Proceedings of the CP90 Conference on Computational Physics*. World Scientific Publishing Co. Singapore, 1991.

[54] O. Sauter, C. Angioni, and Y.R. Lin-Liu. Neoclassical conductivity and bootstrap current formulas for general axisymmetric equilibria and arbitrary collisionality regime. *Physics of Plasmas*,

6(7):2834–2839, 1999.

[55] O. Sauter, C. Angioni, and Y.R. Lin-Liu. Erratum: Neoclassical conductivity and bootstrap current formulas for general axisymmetric equilibria and arbitrary collisionality regime [Phys. Plasmas 6, 2834 (1999)]. *Physics of Plasmas*, 9(12):5140–5140, 2002.

[56] R.L. Miller, M.S. Chu, J.M. Greene, Y.R. Lin-Liu, and R.E. Waltz. Noncircular, finite aspect ratio, local equilibrium model. *Physics of Plasmas*, 5(4):973–978, 1998.

[57] N. Aiba, C. Giroud, M. Honda, E. Delabie, S. Saarelma, L. Frassinetti, I. Lupelli, F.J. Casson, S. Pamela, H. Urano, C.F. Maggi, and JET Contributors. Numerical analysis of ELM stability with rotation and ion diamagnetic drift effects in JET. *Nuclear Fusion*, 57(12):126001, 2017.

[58] N. Aiba, S. Pamela, M. Honda, H. Urano, C. Giroud, E. Delabie, L. Frassinetti, I. Lupelli, N. Hayashi, G. Huijsmans, JET Contributors, and JT-60SA Research Unit. Analysis of ELM stability with extended MHD models in JET, JT-60U and future JT-60SA tokamak plasmas. *Plasma Physics and Controlled Fusion*, 60(1):014032, 2017.

[59] N. Aiba, M. Furukawa, M. Hirota, and S. Tokuda. Destabilization mechanism of edge localized MHD mode by a toroidal rotation in tokamaks. *Nuclear Fusion*, 50(4):045002, 2010.

[60] C. Day. Basics and applications of cryopumps. In *CERN Accelerator School, Vacuum in accelerators, Platja d'Aro, Spain, 16-24 May 2006*, pages 241–274, 2006.

[61] C. Day. Chapter 8 - Use of porous materials for cryopumping. In Hari Singh Nalwa, editor, *Handbook of Surfaces and Interfaces of Materials*, pages 265 – 307. Academic Press, Burlington, 2001.

[62] H. Bufferand, B. Bensiali, J. Bucalossi, G. Ciraolo, P. Genesio, Ph. Ghendrih, Y. Marandet, A. Paredes, F. Schwander, E. Serre, and P. Tamain. Near wall plasma simulation using penalization technique with the transport code SolEdge2D-Eirene. *Journal of Nuclear Materials*, 438:S445 – S448, 2013. Proceedings of the 20th International Conference on Plasma-Surface Interactions in Controlled Fusion Devices.

[63] H. Bufferand, G. Ciraolo, Y. Marandet, J. Bucalossi, Ph. Ghendrih, J. Gunn, N. Mellet, P. Tamain, R. Leybros, N. Fedorczak, F. Schwander, and E. Serre. Numerical modelling for divertor design of the WEST device with a focus on plasma-wall interactions. *Nuclear Fusion*, 55(5):053025, 2015.